Optical and Mechanical Characterization of Thin Membranes for X-ray Lithography

by

Gabrielle M. Owen

Submitted to the Department of Electrical Engineering and Computer Science in partial fulfillment of the requirements for the degree of

Master's of Engineering

at the

MASSACHUSETTS INSTITUTE OF TECHNOLOGY

May 6, 1994

Author _____

Department of Electrical Engineering and Computer Science
May 6, 1994

Certified by _____

Henry I. Smith
Thesis Supervisor

Accepted by _____

F. R. Morgenthaler
Chairman, Department Committee on Graduate Theses

Optical and Mechanical Characterization of Thin Membranes for X-ray Lithography

by

Gabrielle M. Owen

Submitted to the
Department of Electrical Engineering and Computer Science

May 6, 1994

In Partial Fulfillment of the Requirements for the Degree of
Master's of Engineering in Electrical Engineering and Computer Science

Abstract

An optical transmission test and a bulge test were designed and tested as part of an endeavor to improve x-ray mask manufacturing. The thicknesses and indices of refraction of silicon nitride membranes were measured with the optical transmission test, and the results were explained using Malé's graphical method. The residual stress and bulk modulus of silicon nitride membranes and PMMA were measured with the bulge test. The bulge test showed a repeatability error of 3% in residual stress measurements and 6% in bulk modulus measurements. A novel in-situ bulge test for a tungsten sputtering system is proposed for controlling the value of the residual stress of sputtered tungsten.

Thesis Supervisor: Henry I. Smith
Title: Keithley Professor of Electrical Engineering

Optical and Mechanical Characterization of Thin Membranes for X-ray Lithography

by

Gabrielle M. Owen

Submitted to the
Department of Electrical Engineering and Computer Science

May 6, 1994

In Partial Fulfillment of the Requirements for the Degree of
Master's of Engineering in Electrical Engineering and Computer Science

Abstract

An optical transmission test and a bulge test were designed and tested as part of an endeavor to improve x-ray mask manufacturing. The thicknesses and indices of refraction of silicon nitride membranes were measured with the optical transmission test, and the results were explained using Malé's graphical method. The residual stress and bulk modulus of silicon nitride membranes and PMMA were measured with the bulge test. The bulge test showed a repeatability error of 3% in residual stress measurements and 6% in bulk modulus measurements. A novel in-situ bulge test for a tungsten sputtering system is proposed for controlling the value of the residual stress of sputtered tungsten.

Thesis Supervisor: Henry I. Smith
Title: Keithley Professor of Electrical Engineering

Acknowledgements

There are many people who have helped in the production of this thesis. I am indebted to all of my teachers at M.I.T. and at previous schools for helping me to develop my technical skills. I am grateful to my advisor Professor Henry I. Smith for his superb technical guidance and financial support. While busy designing his new lab, Dr. Mark Schattenburg has also enthusiastically guided this research. I would like to thank Scott Hector for his patience in answering my many questions and for his help in preparing a multilayer bulge sample. The technical assistance in the NanoStructures Laboratory also deserves thanks for their outstanding work. Mark Mondol's expert assistance in building the bulge test measurement system was critical to this research. Bob Sisson has been key in fabricating the x-ray masks, and Jimmy Carter has kept the lab running through the many power outages. Many thanks to all of the students in the NanoStructures Lab! I would finally like to thank my family and all of my friends for their continuous support, humor, and understanding. Thanks a bunch everyone!!!

Table of Contents

List of Figures

Chapter 1

Introduction

Lithography, the process of printing images on surfaces, is a key part of semiconductor processing. Presently optical lithography, printing using a near-visible light source, is used in industrial semiconductor manufacturing. X-ray lithography (XRL), printing using an x-ray source, was introduced in 1972 [1] and is expected to replace optical lithography in the near future because of its capability of printing smaller features than optical lithography.[2]

A schematic of proximity x-ray lithography is shown in Figure 1.1. An x-ray mask patterned with an x-ray absorber is illuminated with x-rays passing through a vacuum window. X-rays travel through the transparent mask and expose the x-ray sensitive resist on the silicon wafer. Behind the absorber the x-ray sensitive resist is left unexposed because the illuminating x-rays are attenuated by the absorber. Subsequent development of the resist results in a copy on the substrate of the x-ray mask pattern.

A diagram of an x-ray mask is shown in Figure 1.2. An x-ray mask is a thin membrane, approximately one micron thick, which is typically made of Si, SiNx, SiC, or diamond. [3, 4] A layer of x-ray absorber, thick enough to ensure 5 to 10 dB attenuation of the x-ray source, is deposited on top of the membrane. The x-ray absorber is patterned with the desired pattern via techniques such as e-beam lithography and RIE.

Since x-ray lithography is a one-to-one replication technique, its accuracy is limited by the precision of the features on the original mask. A major concern is that the stress of the x-ray absorber will lead to pattern distortion through deformation of the thin supporting x-ray mask. [5-7] Two types of pattern distortion may be caused by the stress of the x-ray absorber: in-plane distortion and out-of-plane distortion. Stretching and shrinking of the

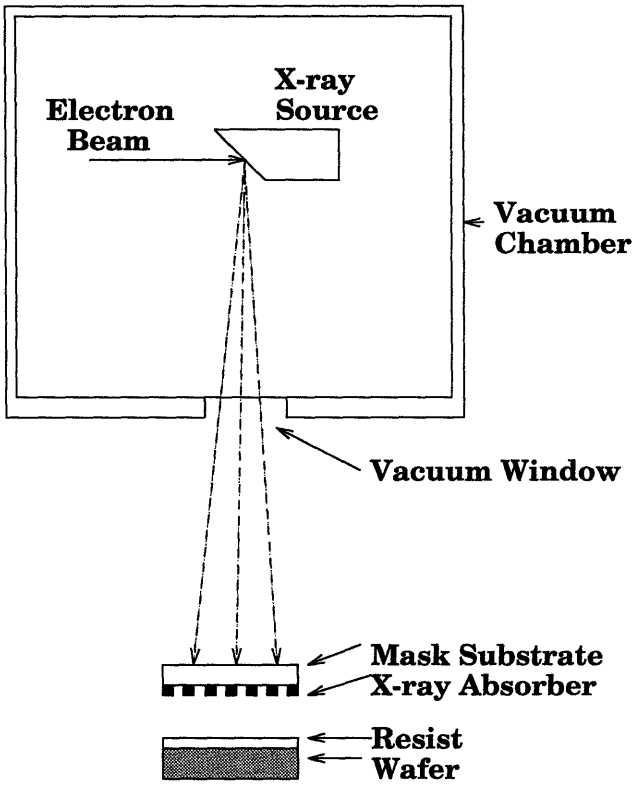

Figure 1.1: X-ray lithography schematic

pattern in the original plane of the membrane results in in-plane distortion. Out-of-plane distortion occurs when the x-ray mask bends out of its original plane. Out-of-plane distortion is negligible when a synchroton source is used, but in-plane distortion is always a concern in x-ray lithography. [7]

This thesis concentrates on improving x-ray mask manufacturing through the development of equipment to test the optical and mechanical properties of x-ray masks. Two tests for x-ray masks are described: an optical transmission test and a bulge test. The optical transmission test is attractive because it provides a non-contact method of measuring the thickness and index of refraction of an x-ray mask or a vacuum window. The thickness of the x-ray mask is needed in the bulge test to calculate the stress and bulk modulus of the sample. The thickness of the vacuum window and membrane determine the amount of x-

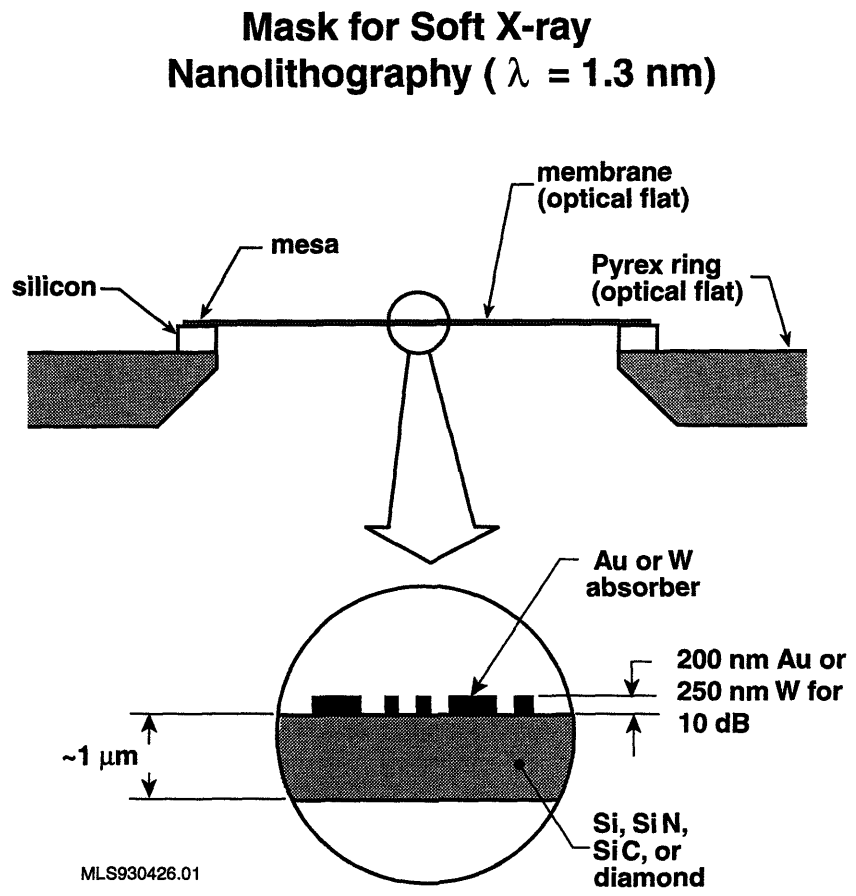

Figure 1.2: X-ray Mask schematic

ray which reaches the silicon wafer as shown in Figure 1.1. The bulge test provides a non-destructive test to determine the intrinsic stresses and bulk moduli of layers of films on an x-ray mask. [8-17] Ideally a membrane should have a high intrinsic stress, and an absorber should have a very low intrinsic stress to minimize pattern distortion. Through knowledge of the optical and mechanical properties of an x-ray mask, quality control is provided on the x-ray mask manufacturing process.

Chapter 2

Reflection and Transmission by a Layered Medium

In this chapter the reflected and transmitted power of the TE component an incident field on a layered medium will be calculated and then the principle of duality will be used to find the solutions for the TM component. [18] The transmitted power from an ambient-film-ambient system will be calculated in terms of the index and thickness of the film and the incident wavelength. The results will be used in Chapter 5 to experimentally find the thickness of a thin film.

A plane wave incident on a medium and the reflected and transmitted waves it produces define the plane of incidence. The incident wave can be completely described by transverse electric (TE) and transverse magnetic (TM) waves.

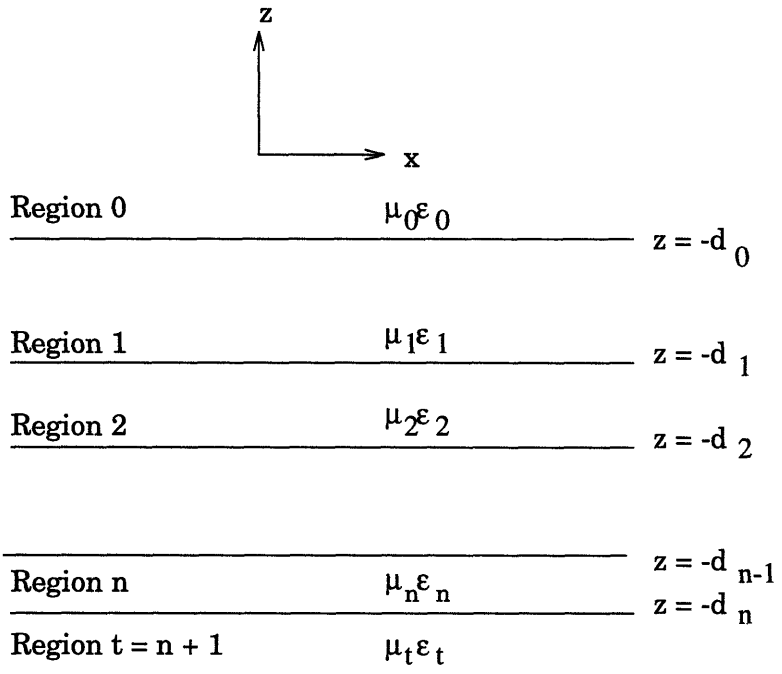

Figure 2.1: Medium with isotropic layers

The electric field vector of TE waves is perpendicular to the plane of incidence, while the magnetic field vector of TM waves is perpendicular to the plane of incidence. The TE and TM components of the incident wave can be analyzed separately through Maxwell's equations.

In Figure 2.1 an isotropic layered medium is shown with each layer described by a permittivity ε_l and a permeability μ_l. An incident TE plane wave in region 0 can be described by $E_y = E_o e^{-ik_z z + ik_x x}$. Assuming the field vectors are dependent on x and z only, Maxwell's equations for TE waves are:

$$H_{lx} = -\frac{1}{i\omega\mu_l}\frac{\partial E_{ly}}{\partial z}$$

$$H_{lz} = \frac{1}{i\omega\mu_l}\frac{\partial E_{ly}}{\partial z} \tag{2.1}$$

$$\left(\frac{\partial^2}{\partial x^2} + \frac{\partial^2}{\partial z^2} + \omega^2\mu_l\varepsilon_l\right)E_{ly} = 0$$

Using Maxwell's equations for TE waves we find the electric and magnetic field vectors in the *l*th layer to be:

$$E_{ly} = (A_l e^{ik_{lz}z} + B_l e^{-ik_{lz}z})\, e^{ik_x x}$$

$$H_{lx} = -\frac{k_{lz}}{\omega\mu_l}(A_l e^{ik_{lz}z} - B_l e^{-ik_{lz}z})\, e^{ik_x x} \tag{2.2}$$

$$H_{lz} = \frac{k_x}{\omega\mu_l}(A_l e^{ik_{lz}z} + B_l e^{-ik_{lz}z})\, e^{ik_x x}$$

where the amplitude A_l corresponds with components travelling in the +z-direction, and the amplitude B_l corresponds with components travelling in the -z-direction. A layer iden-

tification subscript l for k_x is not used since continuity of the tangential electric field at a boundary requires that k_x be the same in each of the layers.

At the boundary $z = -d_l$, boundary conditions require that the tangential electric and magnetic fields are continuous:

$$\begin{aligned} A_l e^{-ik_{lz}d_l} + B_l e^{ik_{lz}d_l} &= A_{l+1} e^{-ik_{(l+1)z}d_l} + B_{l+1} e^{ik_{(l+1)z}d_l} \\ p_{(l+1)l}\left[A_l e^{-ik_{lz}d_l} - B_l e^{ik_{lz}d_l}\right] &= \left[A_{l+1} e^{-ik_{(l+1)z}d_l} - B_{l+1} e^{ik_{(l+1)z}d_l}\right] \end{aligned} \tag{2.3}$$

where for TE waves:

$$p_{(l+1)l} = \frac{\mu_{(l+1)} k_{lz}}{\mu_l k_{(l+1)z}} = \frac{1}{p_{l(l+1)}} \tag{2.4}$$

Solving for A_{l+1} and B_{l+1} and expressing the answer in matrix form, we have:

$$\begin{bmatrix} A_{l+1} e^{-ik_{(l+1)z}d_{(l+1)}} \\ B_{l+1} e^{ik_{(l+1)z}d_{(l+1)}} \end{bmatrix} = \bar{V}_{(l+1)l} \cdot \begin{bmatrix} A_l e^{-ik_{lz}d_l} \\ B_l e^{ik_{lz}d_l} \end{bmatrix} \tag{2.5}$$

where the forward-propagating matrix $\bar{V}_{(l+1)l}$ is:

$$\bar{V}_{(l+1)l} = \frac{1}{2}\left[1 + p_{(l+1)l}\right] \begin{bmatrix} e^{-ik_{(l+1)z}(d_{(l+1)} - d_l)} & R_{(l+1)l} e^{-ik_{(l+1)z}(d_{(l+1)} - d_l)} \\ R_{(l+1)l} e^{ik_{(l+1)z}(d_{(l+1)} - d_l)} & e^{ik_{(l+1)z}(d_{(l+1)} - d_l)} \end{bmatrix} \tag{2.6}$$

$R_{(l+1)l}$ is the reflection coefficient at the boundary between regions $l+1$ and l, where the first subscript is the region with the incident wave. For TE waves the reflection coefficient $R_{(l+1)l}$ is:

$$R_{(l+1)\,l} = \frac{1 - p_{(l+1)\,l}}{1 + p_{(l+1)\,l}} = -R_{l\,(l+1)} \tag{2.7}$$

where $p_{(l+1)l}$ is given in equation (2.4) for TE waves. To determine the wave amplitudes in region $m > l$ in terms of those in any region l the following formula can be used:

$$\begin{bmatrix} A_m e^{-ik_{mz}d_m} \\ B_m e^{ik_{mz}d_m} \end{bmatrix} = \overline{V}_{m\,(m-1)} \cdot \overline{V}_{(m-1)\;(m-2)} \cdots \overline{V}_{(l+1)\,l} \cdot \begin{bmatrix} A_l e^{-ik_{lz}d_l} \\ B_l e^{ik_{lz}d_l} \end{bmatrix} \tag{2.8}$$

where $\overline{V}_{m(m-1)}$ is given in equation (2.6).

When evaluating equation (2.5) between regions n and $t = n+1$, we need to use care since the region t is of infinite thickness. In equation (2.5) we eliminate the common factor $e^{-ik_{(l+1)z}d_{(l+1)}}$ from the top line and the common factor $e^{ik_{(l+1)z}d_{(l+1)}}$ from the bottom line. Also in region t there is no wave propagating in the +z-direction:

$$\begin{aligned} A_t &= 0 \\ B_t &= TE_o \end{aligned} \tag{2.9}$$

Thus between layers n and t equation (2.5) reduces to:

$$\begin{bmatrix} 0 \\ T \end{bmatrix} = \overline{V}_{tn} \cdot \begin{bmatrix} A_n e^{-ik_{nz}d_n} \\ B_n e^{ik_{nz}d_n} \end{bmatrix} \tag{2.10}$$

where

$$\overline{V}_{tn} = \frac{1}{2}(1+p_{tn}) \begin{bmatrix} e^{ik_{tz}d_n} & R_{tn}e^{ik_{tz}d_n} \\ R_{tn}e^{-ik_{tz}d_n} & e^{-ik_{tz}d_n} \end{bmatrix} \tag{2.11}$$

To find the transmission coefficient T in terms of the incident field in region 0, we expand the vector on the right hand side of equation (2.10) by using equation (2.8). In equation (2.8) we set $l = 0$, m = n, $A_t = 0$, $A_0 = R_{01}E_o$, and $B_0 = E_o$ and obtain:

$$\begin{bmatrix} 0 \\ T \end{bmatrix} = \overline{V}_{t0} \cdot \begin{bmatrix} R_{01}e^{-ik_z d_o} \\ e^{ik_z d_o} \end{bmatrix} \tag{2.12}$$

where

$$\overline{V}_{t0} = \overline{V}_{tn} \cdot \overline{V}_{n(n-1)} \cdots \overline{V}_{10} \tag{2.13}$$

In order to find the transmission coefficient T for the TM case, we use the principle of duality, namely we replace $\overline{E}$ by $\overline{H}$, $\overline{H}$ by $-\overline{E}$, and interchange μ and ε. A_l and B_l now denote amplitudes of tangential magnetic fields for TM waves. For TM waves equations (2.7), (2.11), and (2.12) can be used by making the substitution:

$$p_{(l+1)l} = \frac{\varepsilon_{(l+1)}k_{lz}}{\varepsilon_l k_{(l+1)z}} = \frac{1}{p_{l(l+1)}} \tag{2.14}$$

In Figure 2.2 an ambient-film-ambient system is shown with a normally incident k vector. Using equations (2.4), (2.7), (2.11), (2.12), (2.13), and (2.14) we find the transmitted power *t* for both TE and TM waves of the ambient-film-ambient system in terms of the index of the film to be:

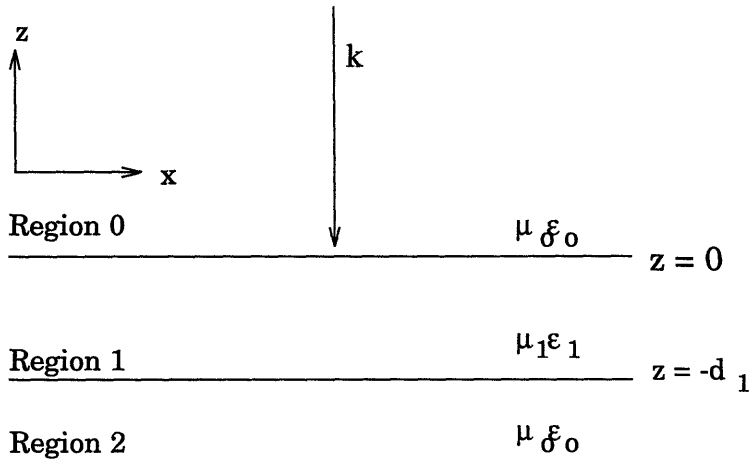

Figure 2.2: Ambient-film-ambient system

$$t = |T|^2 = \left| \frac{4N_1 e^{i2\pi d_1 N_1/\lambda}}{(1+N_1)^2 - (1-N_1)^2 e^{i4\pi d_1 N_1/\lambda}} \right|^2 \tag{2.15}$$

where N_1 is the index of the film. The real and imaginary parts of the index region 1 can be approximated as polynomials as shown in equation (2.16).

$$\begin{aligned} N_1 &= n + i\alpha \\ n &= n_0 + n_2/\lambda^2 + n_4/\lambda^4 \\ \alpha &= \alpha_0 + \alpha_1/\lambda + \alpha_3/\lambda^3 \end{aligned} \tag{2.16}$$

In Chapter 5 the transmitted power of an ambient-film-ambient system will be measured over a broad wavelength range. Equations (2.15) and (2.16) will be used to derive the thickness of the film from the measured transmitted power in Chapter 5.

Chapter 3

Bulge Test

In this chapter the basic concepts of the mechanics of solids will be reviewed before embarking on finding a relationship between the pressure, deflection, residual stresses, and bulk moduli for a multi-layered circular membrane. The overview of solid mechanics includes definitions of basic terms of solid mechanics, Hooke's laws, and the principle of minimum potential energy. [19, 20] The multi-layered circular membrane problem will be solved using the energy-minimization method, and the solution will be used in finding the bulk moduli and residual stresses of single-layer and multi-layer samples in Chapter 5.

3.1 Overview of the Principles of the Solids of Mechanics

3.1.1 Stress

Stress is a vector with dimensions of force per unit area. The stress distribution through an object is generally nonuniform, with regions of low or high stress present. A map of the stress distribution through an object can be made by calculating the local stress at each point using:

$$\bar{\sigma} = \lim_{\delta A \to 0} \left(\frac{\delta \bar{F}}{\delta A} \right) \tag{3.17}$$

where $\bar{\sigma}$ is stress, $\bar{F}$ is force, and A is area. The SI units for stress are N/m^2 which is also called a Pascal. Uniform stress is a special stress distribution case in which the total force is uniformly distributed over a given area. When the stress throughout an object is uniform or varies little, the stress can be described macroscopically as:

$$\bar{\sigma} = \frac{\delta \bar{F}}{\delta A} \tag{3.18}$$

where $\bar{\sigma}$ is stress, $\bar{F}$ is force, and A is area.

Stress is categorized by the direction of the acting force with respect to the material. The force acting on a material is the sum of force components perpendicular and parallel to the surface. Force components perpendicular to the area of contact give rise to normal stresses, and force components parallel to the material cause shear stresses as shown in Figure 3.3. Normal stresses are further divided into tensile and compressive stresses, depending on the direction of the normal force component vector. Tensile stress occurs when the force acts out of the material, and compressive stress occurs when the normal stress acts into the material.

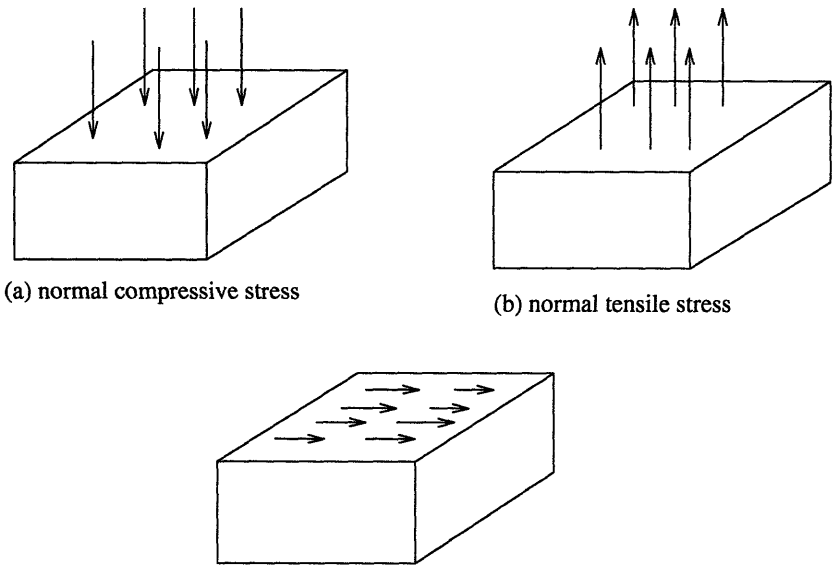

(a) normal compressive stress

(b) normal tensile stress

(c) shear stress

Figure 3.3: Stress types

3.1.2 Strain

When stress is applied to a material which is constrained against moving as a rigid body, a change in the shape of the material occurs. The deformation which occurs when a normal stress is applied to an object is called a *normal* or *direct strain*. The appropriate definition of strain to use depends on the situation encountered. The engineer's strain is widely used in the case of small strains. Engineer's strain ε_i in the i-direction is defined as:

$$\varepsilon_i = \frac{\Delta L_i}{L_i} \tag{3.19}$$

where ΔL_i is the change in length in the i-direction, and L_i is the original length in the i-direction. The sign convention for the change in length is to use a positive sign for an increase in length and a negative sign for a decrease in length.

A material will typically be subjected to normal stresses in more than one direction. The normal stresses on an isotropic material give rise to normal strains, as seen in the generalized Hooke's law (equation (3.24)). The changes in length along each axis alter the total volume of the object. *Volumetric strain* ε_{vol} is the ratio between the change in volume $(V-V_o)$ and the original volume V_o.

$$\varepsilon_{vol} = \frac{V - V_o}{V_o} \tag{3.20}$$

3.1.3 Young's Modulus and Bulk Modulus

Stress and strain are linked by the properties of the material. For uniaxial stress on a linear material only, the relationship between stress and strain in the elastic region is expressed by Hooke's law:

$$\sigma_i = E\varepsilon_i \tag{3.21}$$

where the constant E has the units of stress and is the *modulus of elasticity* of the material or *Young's Modulus*. For hydrostatic loading conditions, a state in which the normal stresses are equal in all directions, the relationship between hydrostatic stress and volumetric strain can be expressed as:

$$\sigma_H = K\varepsilon_{vol} \tag{3.22}$$

where the constant K has the units of stress and is the *bulk modulus* for the material. Equations (3.21) and (3.22) assume that the deformation of the material is small.

Young's Modulus and the bulk modulus of a material can be found experimentally by developing a stress-strain curve. For each stress applied to a material, the strain produced is measured. The slope of the stress-strain curve gives either the Young's Modulus or the bulk modulus of the material, depending on whether the loading conditions are uniaxial or hydrostatic.

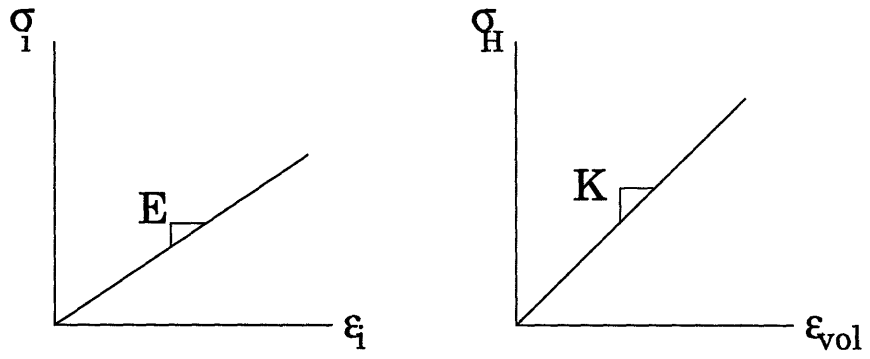

Figure 3.4: Young's modulus and bulk modulus found from stress-strain curves

The stress-strain test gives information about the strength and elasticity of the material in addition to the Young's modulus or bulk modulus. The strength properties of the material determine the maximum level of stresses which can be tolerated in the stress-strain test. The material is considered to be *elastic* if it retraces the original curve to zero stress and strain when the stress is removed. If the original curve back to zero stress and strain is not followed, the yield point has been passed, and a permanent strain or a permanent stress in the material may result.

3.1.4 Poisson's Ratio

A stress along one axis of a material can produce strains along all axes, as seen with rubber bands where an elongation along one axis results in a contraction in the lateral dimensions of the rubber band. The strains for an isotropic material are experimentally found to be:

$$\varepsilon_j = \varepsilon_k = -\upsilon\varepsilon_i = \frac{-\upsilon}{E}\sigma_i \tag{3.23}$$

where ε_i is the strain in the i-direction, E is the Young's modulus, σ_i is the stress in the i-direction, υ is Poisson's ratio, and i, j, and k form an orthogonal cartesian coordinate system. *Poisson's ratio* is the ratio between lateral and axial strain, and it varies between 0 and 0.5, with most metals having a ratio of 0.3.

3.1.5 Generalized Hooke's Law

The generalized Hooke's law for a linear isotropic material states that strain ε_i in the i-direction is the superposition of the effects of the individual stresses in all directions. Two elastic properties of the material, the Young's modulus and the Poisson ratio, link the stresses to the strains produced. The generalized Hooke's law is given below:

$$\begin{aligned}
\varepsilon_x &= \frac{1}{E}\left[\sigma_x - \nu\left(\sigma_y + \sigma_z\right)\right] \\
\varepsilon_y &= \frac{1}{E}\left[\sigma_y - \nu\left(\sigma_z + \sigma_x\right)\right] \\
\varepsilon_z &= \frac{1}{E}\left[\sigma_z - \nu\left(\sigma_x + \sigma_y\right)\right]
\end{aligned} \tag{3.24}$$

where ε_i is the strain, σ_i is the stress, υ is Poisson's ratio, and E is Young's Modulus. The generalized Hookes' law is a linear relation which is valid for small deformations.

3.1.6 Strain Energy

Work is the integral over distance of the dot product of a force vector $\bar{F}$ and a displacement vector $d\bar{s}$. Consider a normal force $\sigma_x dydz$ acting on an area dydz which results in a change in length ε_x dx of a small volume element. Assuming that the relationship between the force and the change in length is linear and no kinetic energy is developed, the work done on the element is the area of the triangle OAB as shown in Figure 3.5. [21] The work dV done is called strain energy and is equal to:

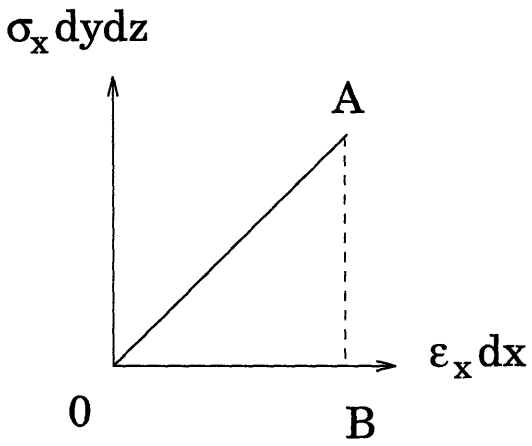

Figure 3.5: Strain energy

$$dV = \frac{1}{2}\sigma_x \varepsilon_x dxdydz \tag{3.25}$$

The total strain energy can be calculated by integrating the strain energy dV of the small volume element over the total volume of the object.

3.1.7 Principle of Minimum Potential Energy

An object constrained against moving as a rigid body will deform when it is under stress. A displacement function can be written which predicts the displacements of the stressed object. The principle of minimum potential energy can be used to ensure that the true displacement function has been chosen. The *principle of minimum potential energy* states that the actual displacement function will make the total potential energy an absolute minimum. [22]

3.2 Calculation of Beam's Equation

In this subsection an equation attributed to Beams [8], which relates the pressure, deflection, residual stress, and Young's modulus of a circular membrane, will be derived. Consider an isotropic, thin-walled spherical membrane subjected to a difference p in hydrostatic pressure between its inner and outer surfaces. The thin-walled condition is met

when the ratio of the thickness of the membrane to the radius of the membrane is less than one-tenth.

Figure 3.6 shows a cross-section of a spherical membrane cut at its equator, with the forces acting on the cut edge found by using Newton's third law, for every action there is an equal and opposite reaction. The forces F_V act at the midpoint of the shell wall, thus

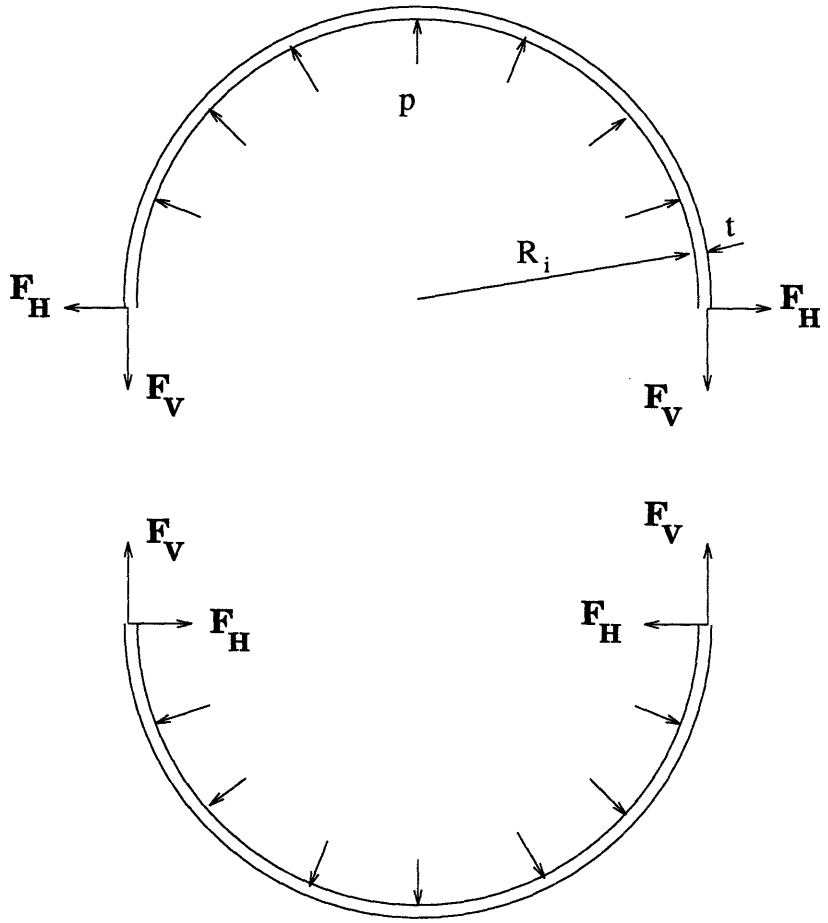

Figure 3.6: Cross-sectional view of the in-plane forces acting on spherical membrane

there is no moment. Rotation of the bottom hemisphere in Figure (3.6) by 180 degrees leads to the conclusion that the forces F_H are equal to zero since they are in opposite direc-

tions in the two hemispheres. The stresses in the θ and φ directions of the membrane are equal since the material is isotropic and its loading conditions are symmetric. The term circumferential stress σ_c will be used to denote stresses in either the θ or φ directions. The circumferential stress is assumed to be uniform throughout the membrane wall.

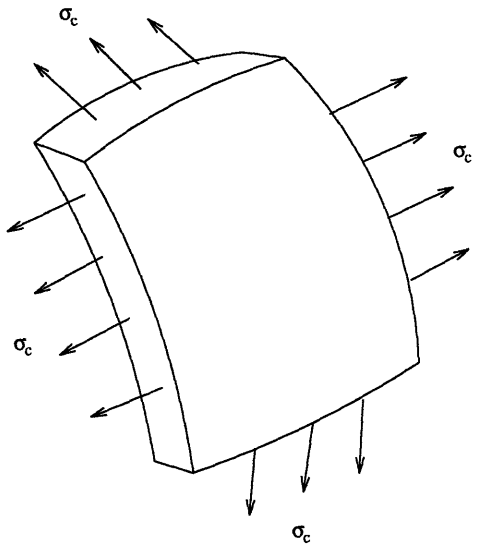

Figure 3.7: Circumferential stress on a volume element of a spherical membrane

The vertical forces on the membrane must balance in a state of equilibrium.The vertical force component F_P related to the internal pressure is:

$$F_P = \int_0^{\pi/2} d\theta \int_0^{2\pi} d\varphi p R_i^2 \sin\theta\cos\theta = \pi p R_i^2 \tag{3.26}$$

where R_i is the inner diameter of the spherical membrane, and p is the differential hydrostatic pressure. The vertical force from the circumferential stress is equal to $F_V = \sigma_c \pi (R_o^2 - R_i^2)$, where R_o is the outer radius of the spherical membrane. Equating the vertical forces, we find:

$$\sigma_c = \frac{pR_i^2}{2tR_m} \approx \frac{pR_i}{2t} \tag{3.27}$$

where the mean radius R_m of the spherical membrane is $(R_o + R_i)/2$, and t is the thickness of the membrane.

By the generalized Hooke's law a membrane with residual stress σ_o has a circumferential strain ε_c of:

$$\varepsilon_c = \frac{(1-\nu)}{E}(\sigma_c - \sigma_o) \tag{3.28}$$

where ε_c is the circumferential strain of the membrane, E is Young's modulus, ν is the Poisson ratio, and σ_o is the residual stress. For a membrane of radius a which undergoes a hemispherical bulge, the circumferential strain ε_c is defined as the change in arclength divided by the original arclength:

$$\varepsilon_c = \frac{R\theta - a}{a} \tag{3.29}$$

where R is the radius of the membrane, and θ is the angle measured from the vertical of the sphere of radius R as shown in Figure 3.8. Assuming the deflections of the membrane are small compared to the radius of the membrane, $R\theta$ can be approximated well by the first terms of a Taylor series expansion:

$$R\theta = R\sin^{-1}\left(\frac{a}{R}\right) \approx a\left(1 + \frac{a^2}{6R^2}\right) \tag{3.30}$$

Through geometric relations R is found to be:

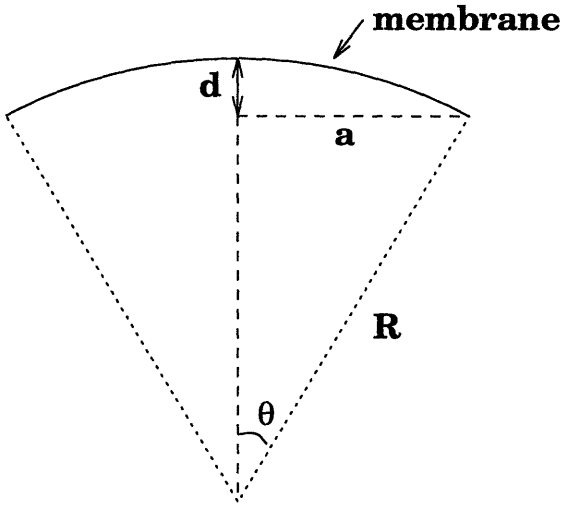

Figure 3.8: Geometry of a bulged membrane

$$R = \frac{a^2}{2d} + \frac{d}{2} \tag{3.31}$$

Assuming the deflection d of the membrane is small, the second term of equation (3.31) can be neglected. Substituting equations (3.30) and (3.31) into equation (3.29), we find the strain of a hemispherically bulged membrane to be:

$$\varepsilon_c = \frac{2d^2}{3a^2} \tag{3.32}$$

Substituting equation (3.32) and equation (3.27) into equation (3.28), we arrive at Beams' equation:

$$\frac{pa^2}{d} = \frac{8t}{3}\left(\frac{E}{1-\nu}\right)\frac{d^2}{a^2} + 4\sigma_o t \tag{3.33}$$

From a plot of pa^2/d versus $(d/a)^2$ the bulk modulus can be extracted from the slope of the plot, and the residual stress can be found from the y-intercept.

3.3 Multi-layer Circular Membrane

In this section the energy minimization approach will be used to calculate a relationship between pressure, deflection, residual stresses, and the bulk moduli of a multi-layered circular membrane. [13] Figure 3.9 is a flow diagram of the procedure which will be used

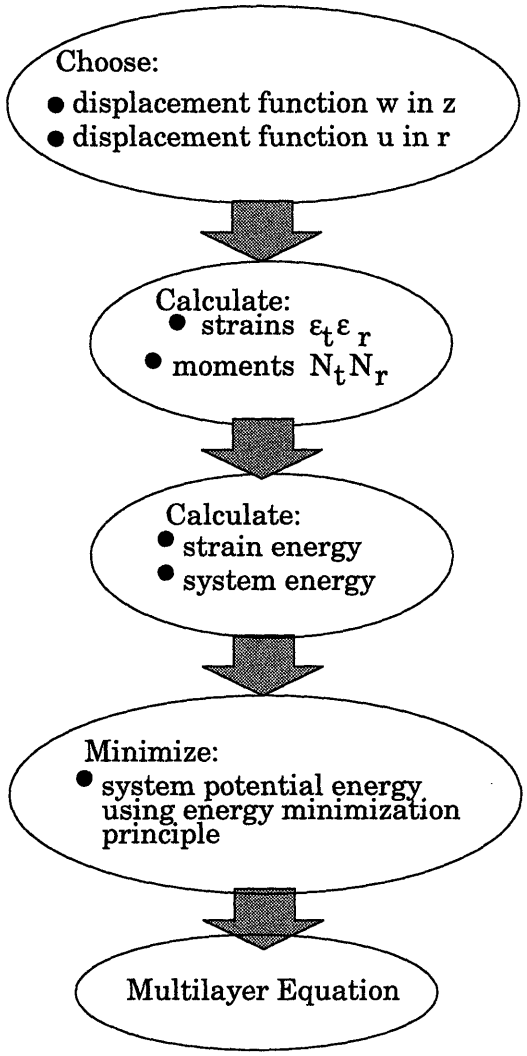

Figure 3.9: Procedure for developing the multilayer equation

to find the multilayer equation. The first step is to choose the displacement function w in the z-direction to be a hemispheric function.

$$w = (R^2 - r^2)^{1/2} - (R - d) + \sum_{k=1}^{m-1} t_k \tag{3.34}$$

where w is the deflection in the z-direction, R is the radius of curvature of the deflected membrane, r is the radial position on the membrane, d is the deflection at the center of the membrane, and t_k is the thickness of the kth layer of the m-layer sample. Assuming (r/R)^2<<1 equation (3.34) can be approximated with the first terms of its Taylor expansion:

$$w = R\left(1 - \frac{r^2}{2R^2} - \frac{r^4}{8R^4} - \ldots\right) - (R - d) + \sum_{k=1}^{m-1} t_k \tag{3.35}$$

Substituting the value of R from equation (3.31) into equation (3.35) we find:

$$w = d\left(1 - \frac{r^2}{a^2}\right) + \sum_{k=1}^{m-1} t_k \tag{3.36}$$

The displacement function u in the r-direction is chosen to be:

$$u = r(a - r)\ (k_1 + k_2 r + \ldots) \tag{3.37}$$

where k_1 and k_2 are constants to be determined through use of the principle of minimum potential energy. The choice of u satisfies the boundary conditions that the radial displacement be zero at the center of the membrane and at the edges of the membrane. Now we calculate the strains in the r-direction and in the transverse direction. [23]

$$\varepsilon_r = \frac{du}{dr} + \frac{1}{2}\left(\frac{dw}{dr}\right)^2 = k_1 a + 2(k_2 a - k_1) r - 3k_2 r^2 + \frac{2d^2 r^2}{a^4}$$
$$\varepsilon_t = \frac{u}{r} = (a - r)\ (k_1 + k_2 r) \tag{3.38}$$

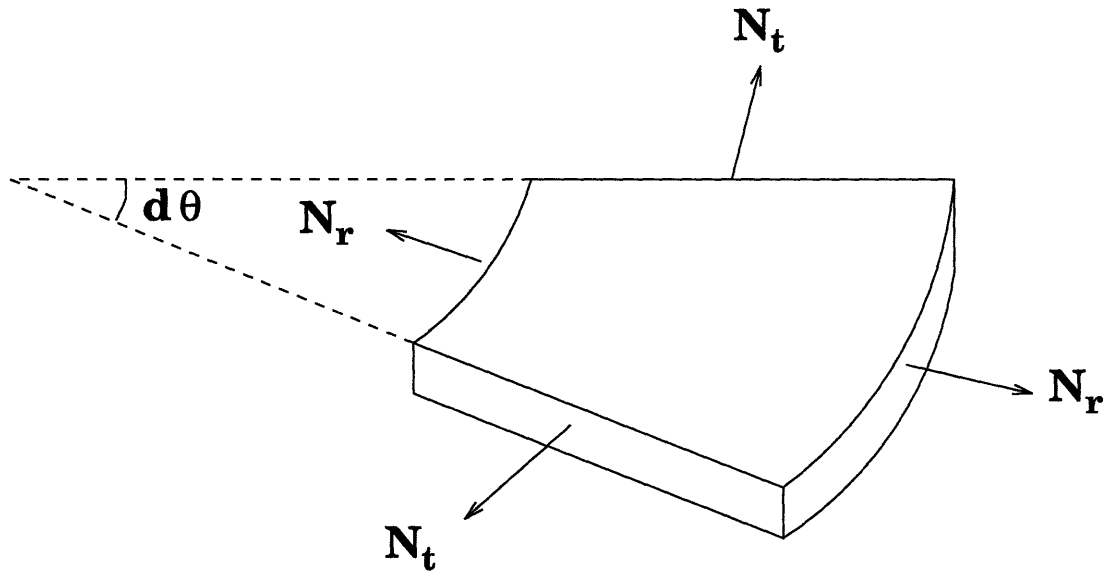

Figure 3.10: Forces on a section of a membrane

Algebraic manipulation of the generalized Hooke's law (3.24) gives:

$$N_r = \sum \frac{E_i t_i}{1-\nu_i^2}(\varepsilon_r + \nu_i \varepsilon_t)$$
$$N_t = \sum \frac{E_i t_i}{1-\nu_i^2}(\varepsilon_t + \nu_i \varepsilon_r) \tag{3.39}$$

where N_r and N_t are the force per unit length in the radial and transverse directions respectively as shown in Figure 3.10, E is Young's modulus of the ith layer, t_i is the thickness of the ith layer, and ν_i is the Poisson ratio of the ith layer. The total force per unit length along the plane of the membrane is the sum of the elastic and residual components:

$$N_r^{total} = N_r + \sum t_i \sigma_i$$
$$N_t^{total} = N_t + \sum t_i \sigma_i \tag{3.40}$$

where N_r^{total} and N_t^{total} are the total force per unit length in the radial and transverse directions respectively, t_i is the thickness of the ith layer of the sample, and σ_i is the residual stress of the ith layer of the sample. The total strain energy V is given by:

$$V = \frac{1}{2}\int_A (N_r^{total}\varepsilon_r + N_t^{total}\varepsilon_t)\, r dr d\theta \tag{3.41}$$

Substituting equations (3.38), (3.39), and (3.40) in (3.41) the total strain energy V is:

$$V = \sum \frac{E_i \pi t_i}{1-\nu_i^2}\left[\int_0^a (\varepsilon_r^2 + \varepsilon_t^2 + 2\nu_i \varepsilon_r \varepsilon_t)\, r dr d\theta\right] + \sum \pi \sigma_i t_i \left[\int_0^a \varepsilon_r + \varepsilon_t r dr\right] \tag{3.42}$$

The total strain energy is the sum of a term due to the elastic stretching process without consideration for the material properties of the membrane and a term due to the residual stress of the membrane.

$$V = V_{ela} + V_{res} \tag{3.43}$$

Upon integration the elastic term V_{ela} is:

$$V_{ela} = \pi \sum \frac{E_i t_i}{1-\nu_i^2}\left(\frac{k_1^2 a^4}{4} + \frac{3k_1 k_2 a^5}{10} + \frac{7k_2^2 a^6}{60} + \frac{-3k_1 a d^2}{5} + \frac{-2k_2 a^2 d^2}{5} + \frac{2d^4}{3a^2}\right) + \pi \sum \frac{E_i t_i \nu_i}{1-\nu_i^2}\left(\frac{k_1 a d^2}{5} + \frac{2k_2 a^2 d^2}{15}\right) \tag{3.44}$$

The residual term is:

$$V_{res} = \pi d^2 \sum \sigma_i t_i \tag{3.45}$$

The principle of minimum potential energy states that the potential energy of a system in equilibrium is a minimum. The total system potential energy V_{sys} is $V_{sys} = V - \int_A P w r dr d\theta$.

$$\frac{\partial V_{sys}}{\partial k_1} = \frac{\partial V_{sys}}{\partial k_2} = 0$$
$$\frac{\partial V_{sys}}{\partial d} = 0 \tag{3.46}$$

The first line of equation (3.46) allows us solve for k1 and k2.

$$k_1 = \frac{d^2}{4a^3}\left(3 - \frac{\sum \frac{E_i \pi t_i \nu_i}{1-\nu_i^2}}{\sum \frac{E_i \pi t_i}{1-\nu_i^2}}\right) \qquad k_2 = \frac{d^2}{4a^4}\left(3 - \frac{\sum \frac{E_i \pi t_i \nu_i}{1-\nu_i^2}}{\sum \frac{E_i \pi t_i}{1-\nu_i^2}}\right) = \frac{k_1}{a} \tag{3.47}$$

Substituting equations (3.44), (3.45), and (3.47) into equation (3.43), we obtain an expression for the total strain energy in terms of the membrane's material properties and geometric properties under deflection, and the pressure of the gas.

$$V = \frac{d^4}{24a^2} f(\nu) + \pi d^2 \sum \sigma_i t_i \tag{3.48}$$

where f(v) is:

$$f(\nu) = \left(7\sum \frac{E_i t_i}{1-\nu_i^2} + 6\sum \frac{E_i t_i \nu_i}{1-\nu_i^2} - \frac{\left(\sum \frac{E_i \pi t_i \nu_i}{1-\nu_i^2}\right)^2}{\sum \frac{E_i \pi t_i}{1-\nu_i^2}}\right) \tag{3.49}$$

The second line of equation (3.46) requires that:

$$\frac{\partial V}{\partial d} = \frac{\pi P a^2}{2} \tag{3.50}$$

Substituting equation (3.48) into equation (3.50), we find a relation between the pressure of the gas, and the membrane's material properties and geometric properties under deflection:

$$P = \frac{d^3}{3a^4} f(\nu) + \frac{4d}{a^2} \sum \sigma_i t_i \tag{3.51}$$

If the Poisson ratio is the same among the layers, equation (3.49) reduces to:

$$f(\nu) = \sum \frac{E_i t_i (7-\nu)}{(1-\nu)} \tag{3.52}$$

and

$$\frac{Pa^2}{d} = \frac{(7-\nu)}{3} \left(\frac{d^2}{a^2}\right) \sum \frac{E_i t_i}{(1-\nu)} + 4 \sum \sigma_i t_i \tag{3.53}$$

In Chapter 5 single and double-layered samples will be pressurized and the resulting deflections will be measured. For a single-layered circular membrane the residual stress and bulk modulus can be found from the y-intercept and slope of a (Pa^2/d) versus $(d/a)^2$ plot, and the thickness t_1 of the membrane:

$$\begin{aligned} \text{residual\_stress1} &= \sigma_1 = \frac{\text{y-intercept}}{4t_1} \\ \text{bulk\_modulus1} &= \frac{E_1}{1-\nu} = \frac{3 \times \text{slope}}{t_1 (7-\nu)} \end{aligned} \tag{3.54}$$

The bulk modulus and residual stress of the second-layer of a double-layered sample can be found with the knowledge of the single-layer parameters, the slope and intercept of the double-layered (Pa^2/d) versus $(d/a)^2$ plot, and the thickness t_2 of the second layer:

$$\text{residual\_stress2} = \sigma_2 = \frac{1}{t_2}\left(\frac{\text{y-intercept}}{4} - \sigma_1 t_1\right)$$

$$\text{bulk\_modulus2} = \frac{E_2}{1-\nu} = \frac{1}{t_2}\left(\frac{3 \times \text{slope}}{(7-\nu)} - \frac{E_1 t_1}{(1-\nu)}\right) \tag{3.55}$$

Equations (3.54) and (3.55) will be used in Chapter 5 to evaluate the residual stresses and bulk moduli of experimental data.

Chapter 4

Experimental Procedure

4.1 Membrane Fabrication

The silicon nitride membrane fabrication process is shown in Figure 4.1. Silicon wafers were coated with silicon-rich, low-stress, LPCVD silicon nitride in the Integrated Circuits laboratory at M.I.T. All subsequent steps were performed in the NanoStructures laboratory at M.I.T. The silicon nitride on the backside of the wafer was RIE etched, and the wafer was cleaved into quarters. The quarter wafer was anodically bonded to an optically flat pyrex ring, and a frontside mesa stencil RIE etch was performed to remove excess silicon nitride. A backside KOH etch-through and frontside mesa etch were done to remove the silicon. Finally the frontside overhang of silicon nitride was removed with Scotch tape.

4.2 Spectrometer Thickness Measurements by Transmission

The setup for the spectrometer thickness measurements is shown in Figure 4.2. The tungsten lamp of an Acton Research Model TDS-429 Dual Light Source was used as the source. An Oriel f/3 fused-silica plano-convex lens collimated the light from the source, and an Oriel laser quality, Al(MgF_2)-coated mirror directed the beam into the entrance slit of the spectrometer. An EG&G 1235 Digital Triple Grating Spectrograph with a blazed grating of 0.5 micron blaze wavelength and spacing of 150 grooves/mm separated the incident light into its spectral orders. An EG&G Model 1453A Silicon Photodiode Detector measured the spectral orders. An EG&G Model 1471A Detector Interface interfaced the spectrograph with a Macintosh computer, and MacOMA 2.55 software was used to acquire the spectra.

The lens and the mirror positions were adjusted to collimate the source light and to direct the light into the entrance slit of the spectrograph respectively. The grating position

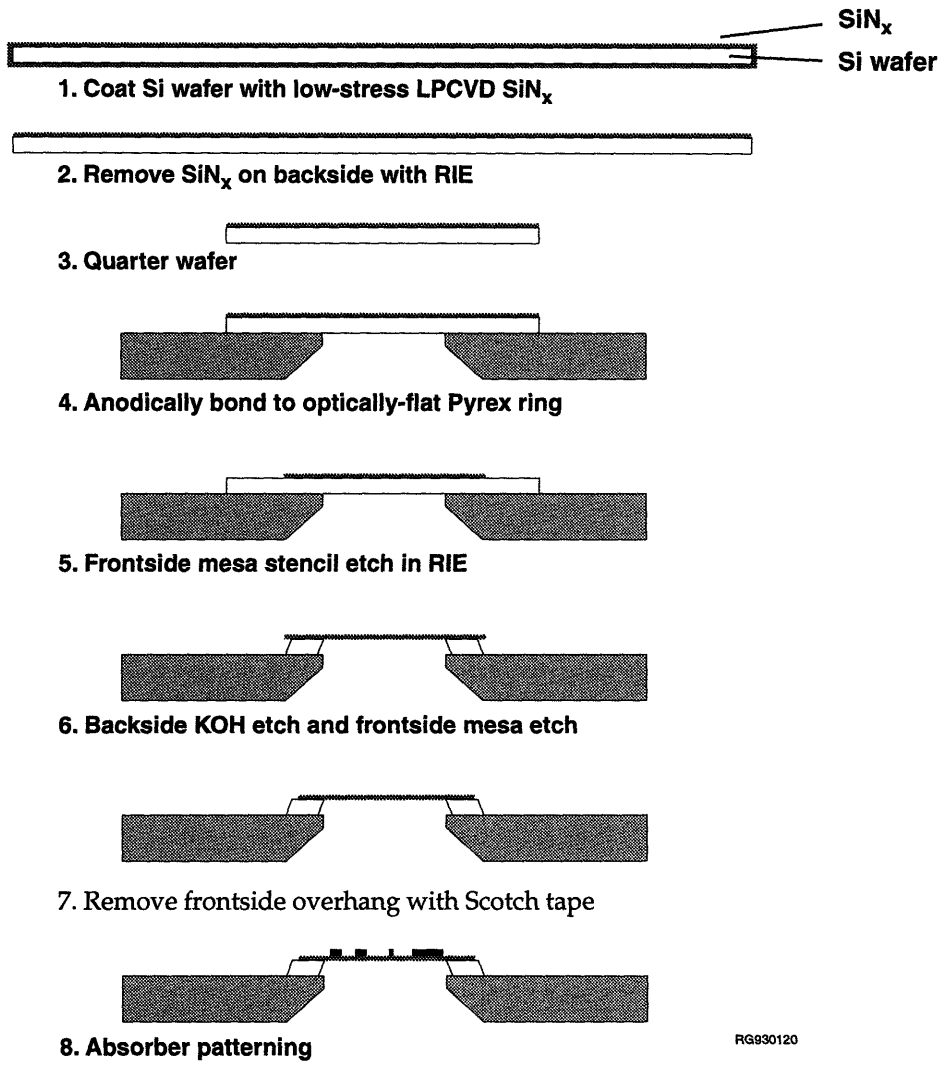

Figure 4.1: Membrane Fabrication Process

was adjusted so the center wavelength of the photodiode array was 700 nm. A calibration curve to correspond the position on the photodiode detector with wavelength was made by using three reference sources: a sodium lamp, a green lamp, and a He-Ne laser. A spectrum of the tungsten light source was taken and saved in computer memory. A silicon nitride membrane was placed on the sample holder, and another spectrum was taken. The spectrum with the sample membrane in place was divided by the spectrum of the light source, resulting in a plot of the transmittance of the membrane versus wavelength.

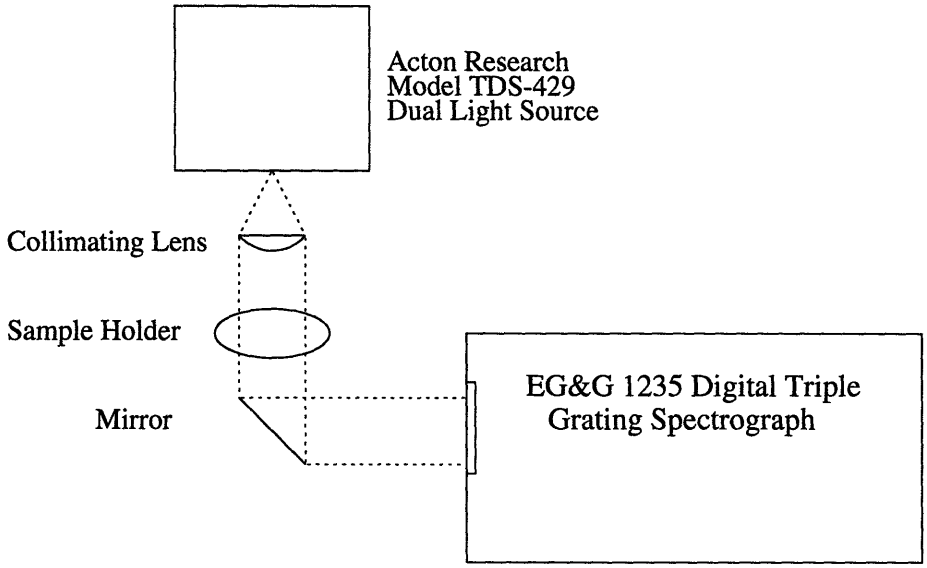

Figure 4.2: Spectrometer Transmission Measurement Setup

The transmittance spectrum was fit to the equation (2.15) using a program written in MATLAB, which can be found in Appendix A. The MATLAB program used the Levenberg-Marquardt least squares curve fitting routine to find the thickness, and real and imaginary parts of the index of refraction versus wavelength. Plots were made of the fit to the spectrum, the real part of the index of refraction versus wavelength, and the imaginary part of the index of refraction.

4.3 Bulge Test Measurements

A schematic of the bulge test chuck is shown in Figure 4.3. The holder is made of aluminum with an inset in the shape of an x-ray mask. The membrane is pressurized by nitrogen gas which enters a drilled passage on the side of the chuck and exits through a small hole in the top of the chuck. The clamping ring made of Ultem is somewhat flexible, allowing the applied stress to be more evenly distributed over the pyrex ring of the x-ray mask.

A schematic of the bulge test measurement setup is shown in Figure 4.4. A program written in LabVIEW was used to control data acquisition and to analyze the data. An MKS

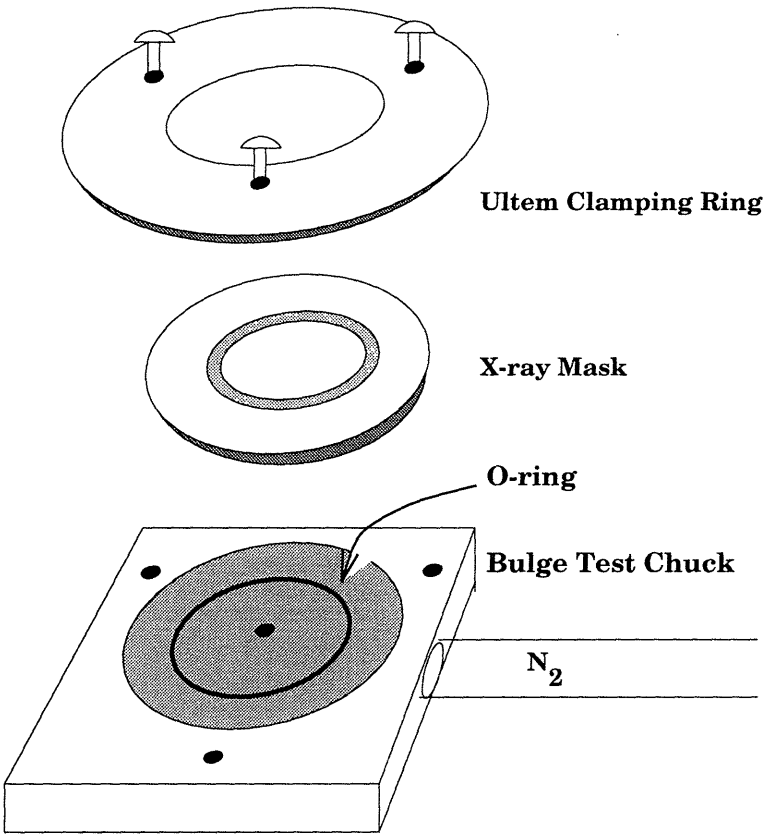

Figure 4.3: Bulge Test Chuck

type 250 proportional controller was used in conjunction with an MKS type 248 control valve and an MKS type 220 capacitance manometer to set the desired pressure within the bulge test chuck chamber and to send the measured value of the chamber pressure to the Macintosh iivx computer. The deflection of the membrane was measured by an MTI-1000 Fotonic sensor which was also interfaced with the computer. The position of the Fotonic sensor was controllable with micrometers in the x, y, and z directions.

The mask was placed in the bulge test holder after the pressure setpoint was checked to be near zero. In order to ensure that the clamping pressure was distributed equally over the pyrex ring of the mask and that no masks were broken, each of the three screws attaching the clamping ring to the bulge test holder was alternately incrementally tightened until

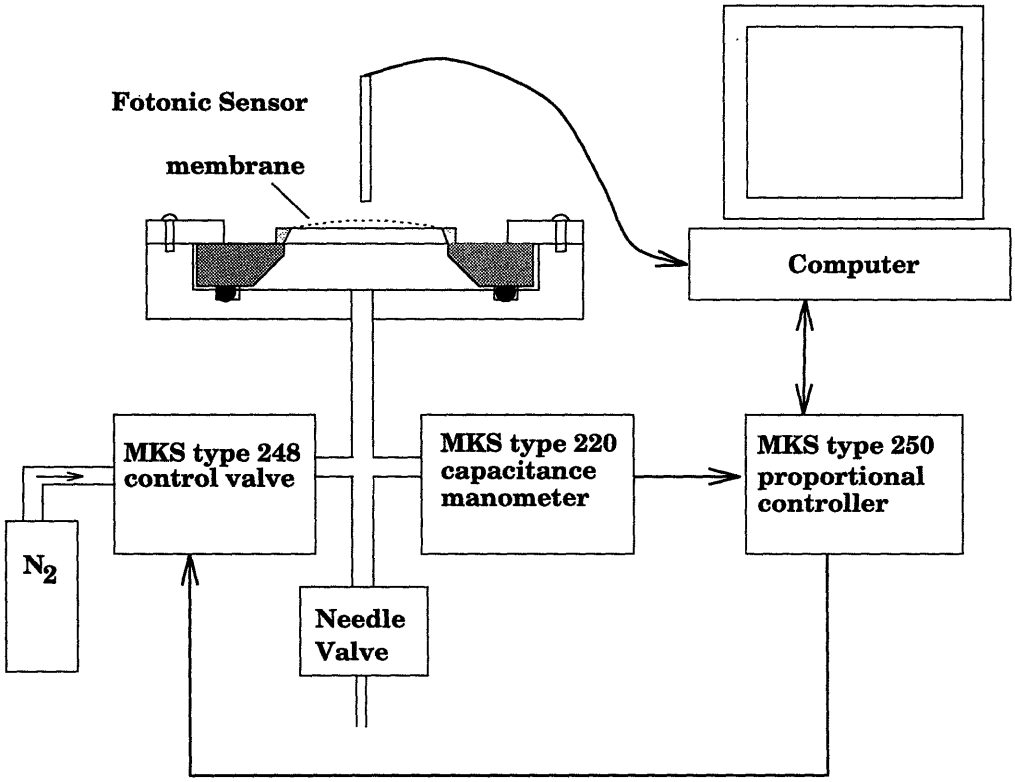

Figure 4.4: Bulge test measurement setup

the force on each screw was 16 oz. in., as read on a torque wrench. The Fotonic sensor was calibrated by moving it toward the sample membrane and by setting its optical peak to 10 Volts. The Fotonic sensor was moved away from the sample until the readout was 7.8 Volts, ensuring that only the linear part of the backslope of the Fotonic sensor calibration curve would be used while deflecting the membrane.

A program written in LabVIEW, which is included in Appendix B, was used to control the data acquisition and the pressure of the gas on the membrane. In all of the bulge testing experiments, the following procedure was used to find the center of the membrane. The single or multilayered sample was first bulged up to approximately 10 torr by increments of 2.5 torr, and the Fotonic sensor position and final deflection were noted. The Fotonic sensor was moved, the sample was bulged again to approximately 10 torr by increments of

2.5 torr, and the new final deflection was noted. The procedure was repeated until a highest final deflection was found, with the surrounding points measuring a lower final deflection.

Three types of single-layer bulge measurements were done: a single-layer bulge test, a single-layer repeatability test, and a single-layer elasticity test. In the single-layer bulge test the membrane was incrementally bulged to a final pressure of 12-20 torr. The slope and intercept of a plot of Pa^2/d versus $(d/a)^2$ were found, where P is the pressure of the gas, a is the radius of the membrane, and d is the deflection of the membrane. The residual stress and bulk modulus of the membrane were found by using equation (3.54) assuming $\nu = 0.28$ and using thickness measurements of the membrane obtained with the optical transmission test.

The single-layer repeatability test and elasticity test are based on the single-layer bulge test. In the single-layer repeatability test, the single-layer bulge test was repeated several times. The membrane was removed from the bulge test chuck in between runs, and the center of the membrane was found on each trial. In the single-layer elasticity test the membrane was incrementally bulged to a final pressure of 12-20 torr, and then the pressure was incrementally decreased. The residual stress and bulk moduli of the membrane were found for the increasing pressure part of the run and the decreasing pressure part of the run by the same procedure as in the single-layer bulge test.

In the multilayer bulge test, a single-layer bulge test was first performed, and the residual stress and bulk modulus of the membrane were found. A layer of 9% PMMA was spun at 3.5 Krpm for 60 seconds, and the sample was subsequently baked for 1 hour at 180 degrees Celsius. The cooled sample was placed in the bulge test chuck, and the pressure on the membrane was incrementally increased. The slope and intercept of a plot of Pa^2/d versus $(d/a)^2$ were found. A step-edge was made on the sample by exposing part of the

PMMA for 45 minutes using a UV lamp with a wavelength of 220 nm, developing until clear in a 2:3 volume ratio of MIBK:IPA, and then rinsing in IPA for 30 seconds. The thickness of the PMMA layer was found by performing a step-edge test under a Linnik interferometer. Equation (3.55) was then used to derive the residual stress and bulk modulus of the PMMA layer assuming ν was equal to 0.28.

Chapter 5

Results

5.1 Optical Transmission Test

Figure 5.1 shows a plot of the transmittance of the silicon nitride x-ray mask MITa076. The graph exhibits seven peaks between 400 and 1000 nm. Above 900 nm the transmittance data is noisier than at lower wavelengths. The width, and the transmittance at the maxima and minima of the peaks increase as wavelength increases. The transmittance at the maxima and minima of the peaks increases rapidly between 400 and 600 nm, and levels off at wavelengths greater than 700 nm. A Levenberg-Marquardt least squares fit to equation (2.15) yielded a measured thickness of 992 nm. The IC laboratory at M.I.T. reported a value of approximately 1 micron for the silicon nitride at deposition (See "Membrane Fabrication Process" on page 35.).

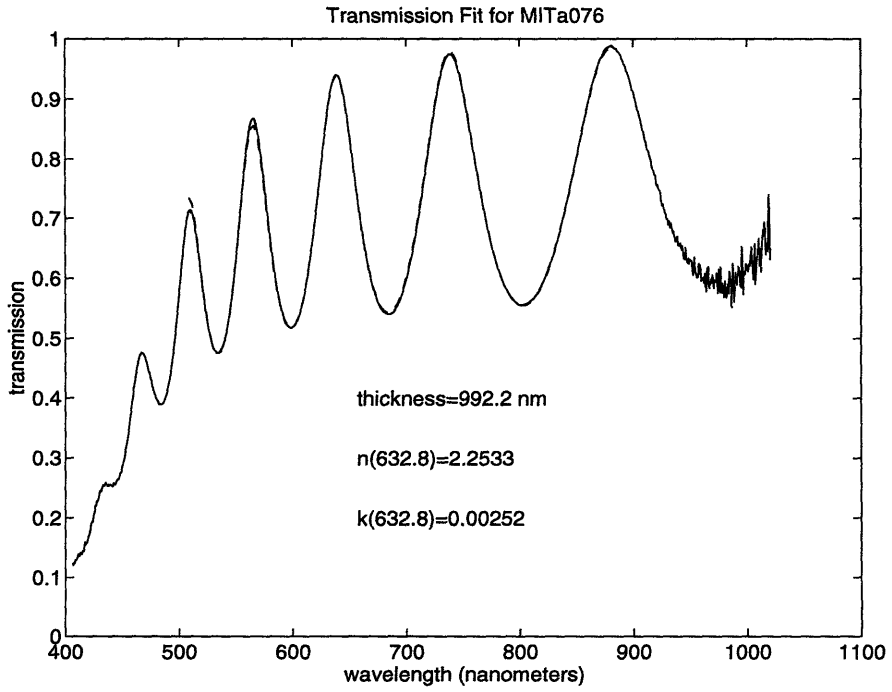

Figure 5.1: Transmittance of MITa076 versus wavelength plus curve fit

In Figures 5.2 and 5.3 the real and imaginary parts of the refractive index of the silicon nitride membrane MITa076 are plotted from the parameters found through the curve fit to the data in Figure 5.1. Both the real and imaginary parts of the refractive index are highest at 400 nm and decrease sharply in the 400 to 600 nm region. The change in value is greater for the real part of the refractive index, which varies from 2.213 to 2.425. The imaginary part of the refractive index remains very small (~ 2E-3 to 30E-3) throughout the 400 to 1000 nm wavelength range. The measured value of the real part of the refractive index at 632.8 nm was 2.26. Ellipsometry measurements by Foxboro of silicon nitride made with different deposition conditions was 2.2. [16]

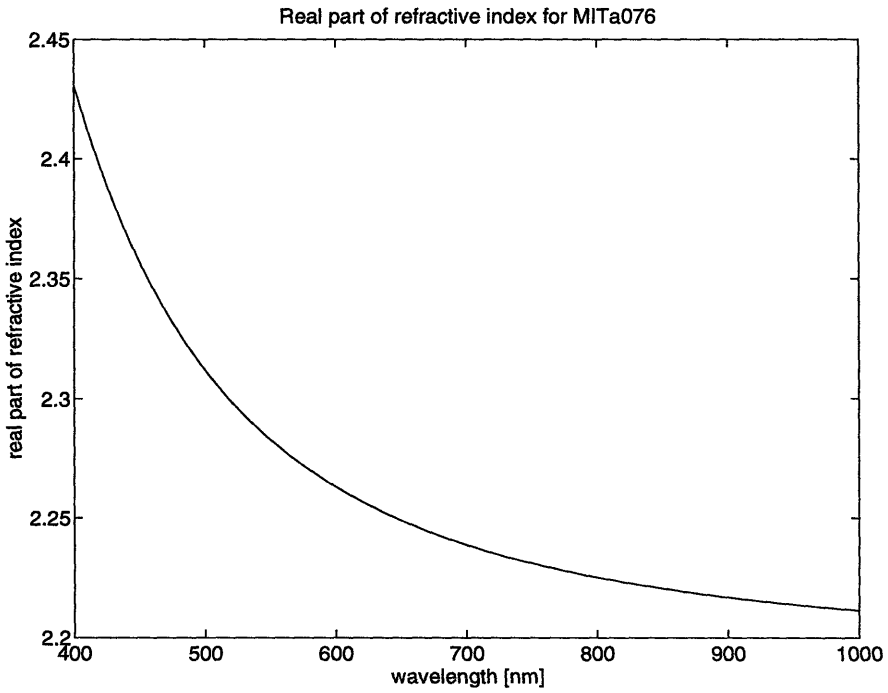

Figure 5.2: Real part of the refractive index of MITa076 versus wavelength

5.2 Bulge Test Measurements

In Figure 5.4 the pressure versus deflection of the silicon nitride x-ray mask MITa203 is plotted. From a deflection value of 0 to 125 microns the pressure-deflection curve is lin-

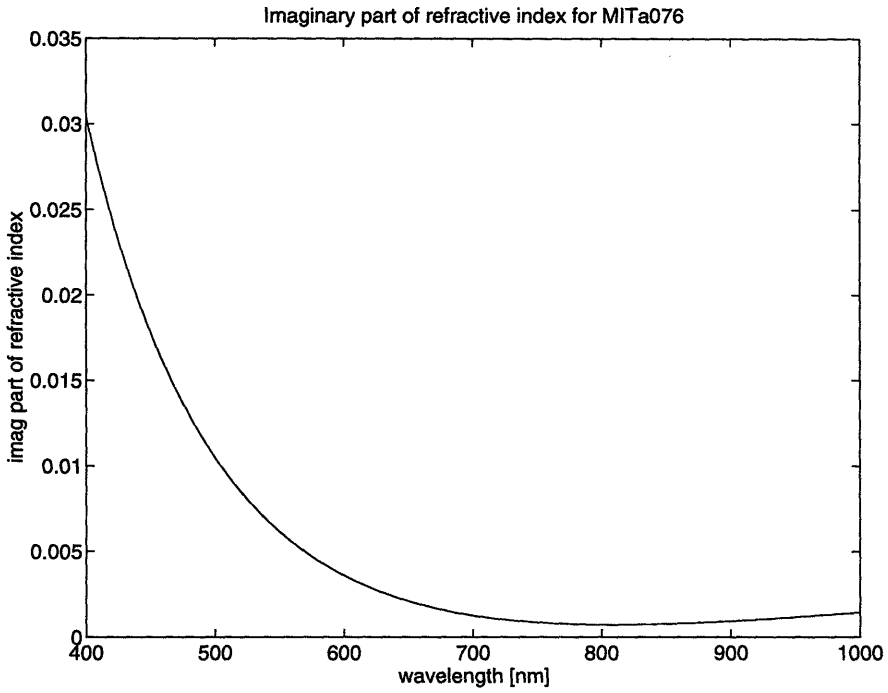

Figure 5.3: Imaginary part of the refractive index of MITa076 versus wavelength

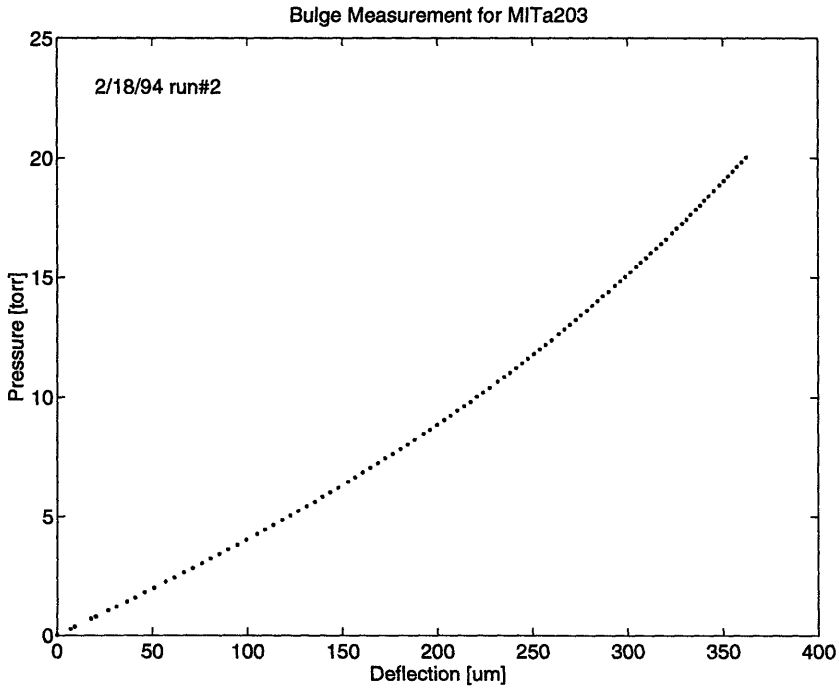

Figure 5.4: Bulge pressure-deflection curve for MITa203

ear. Above a deflection value of 125 microns the pressure-deflection curve is nonlinear. At 20 torr the membrane deflection value is approximately 370 microns. The plot used to derive the residual stress and bulk modulus of MITa203 is shown in Figure 5.5. Using a

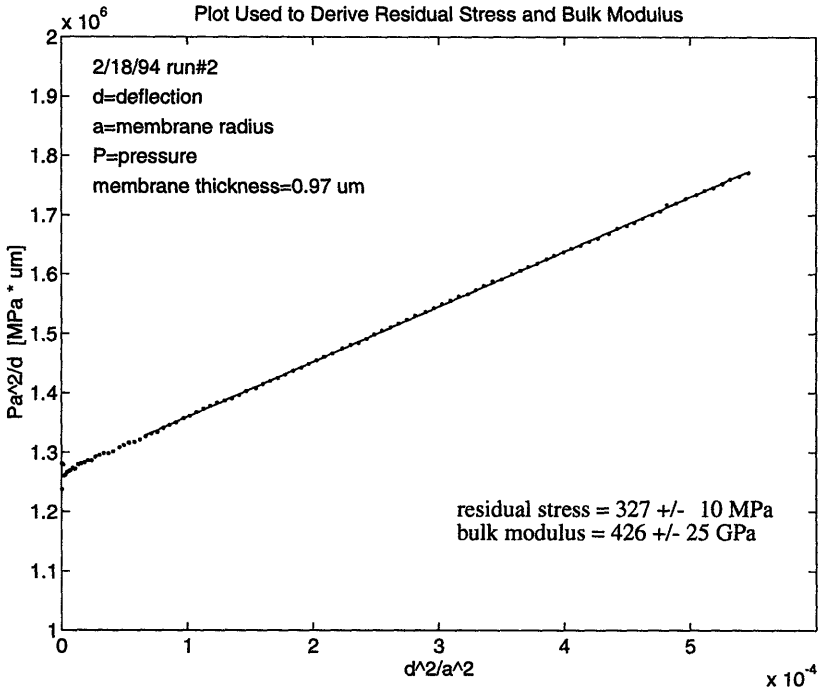

Figure 5.5: Plot used to derive residual stress and bulk modulus of MITa203

linear fit and equation (3.54), a residual stress of 327 +/- 10 MPa and a bulk modulus of 426 +/- 25 GPa were found for MITa203. The errors noted are from the repeatability test shown in Figures 5.7 and 5.8.

In Figure 5.6 the pressure-deflection curve for a Si wafer bonded to a pyrex ring is shown. There is some scatter in the measured data. The measured deflections range from 0 to 7.7 microns in submicron intervals. The pressure-deflection curve is linear throughout the pressure range of 0 to 20 torr. No nonlinear behavior is observed as was seen in the case of the silicon nitride membrane MITa203 shown in Figure 5.4.

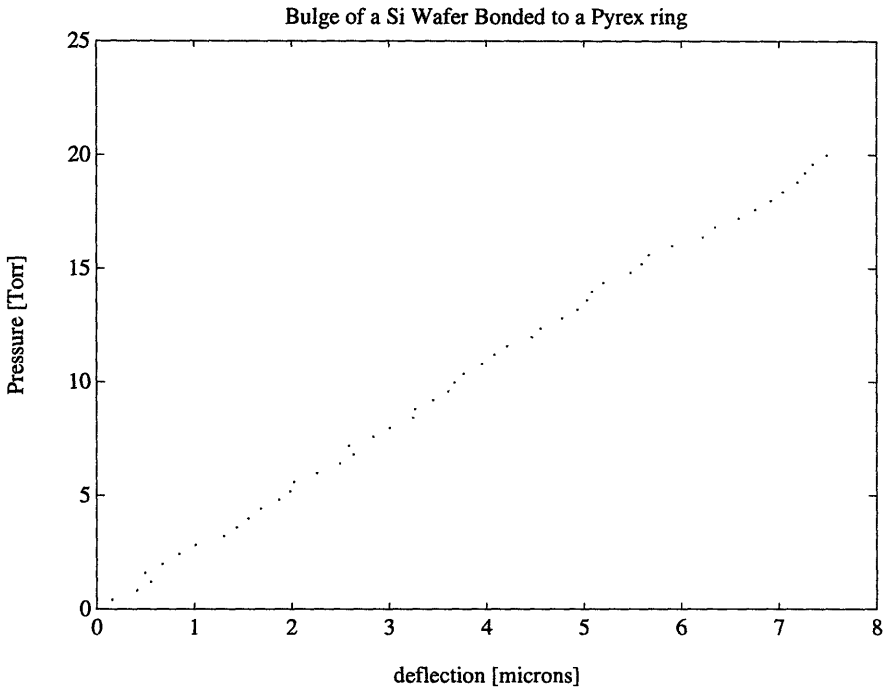

Figure 5.6: Bulge Pressure-Deflection curve for a Si wafer bonded to a pyrex ring

The results of a test of the repeatability of measurements of the residual stress and the bulk modulus of a silicon nitride membrane are shown in Figures 5.7 and 5.8. The residual stress and bulk modulus of MITa203 were measured eleven times. The value obtained for the residual stress was 325 +/- 10 MPa, a 3% error. The measured bulk modulus was 418 +/- 25 GPa, a 6% error. The repeatability error includes the variation in clamping conditions of the sample to the bulge test holder, positioning of the Fotonic sensor, pressure offset errors, and variation of the environment.

In Figure 5.9 a pressure-deflection plot for MITa285 is shown, where the plotted values are from increasing the pressure from zero to 20 torr and then decreasing the pressure back to zero. The measured points from both halves of the run fall on top of each other. In Figure 5.10 the plots used to derive the residual stress and bulk modulus of MITa285 show a slight deviation between the two halves of the run. The calculated residual stress from

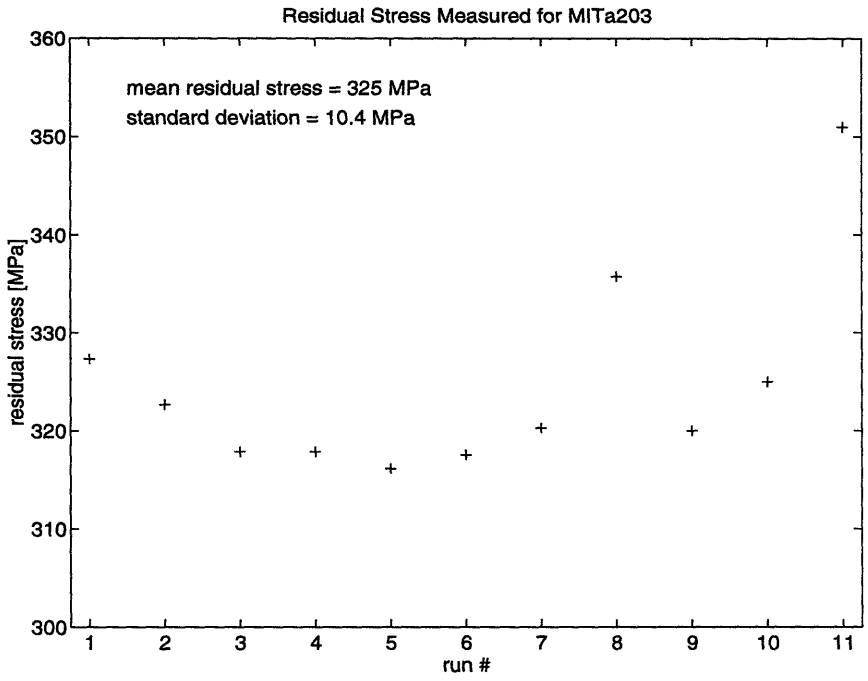

Figure 5.7: Test of the repeatability of residual stress measurements for MITa203

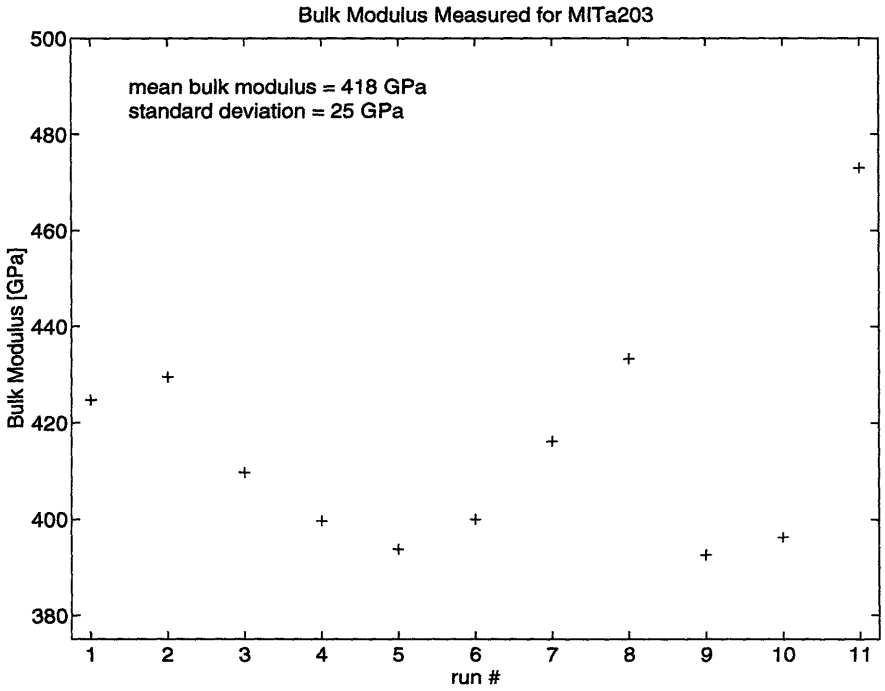

Figure 5.8: Test of the repeatability of bulk modulus measurements for MITa203

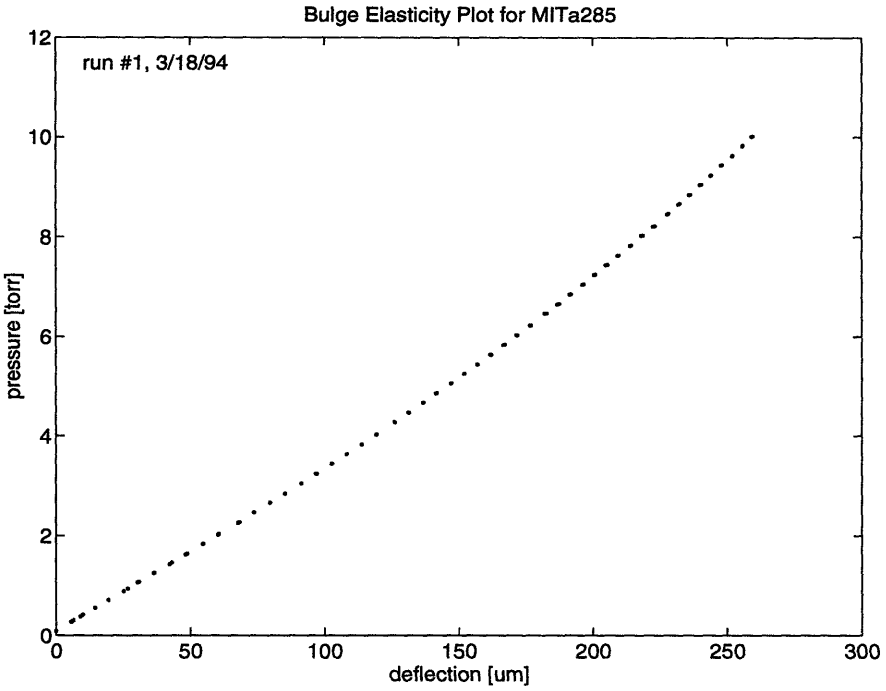

Figure 5.9: Bulge elasticity plot for MITa285

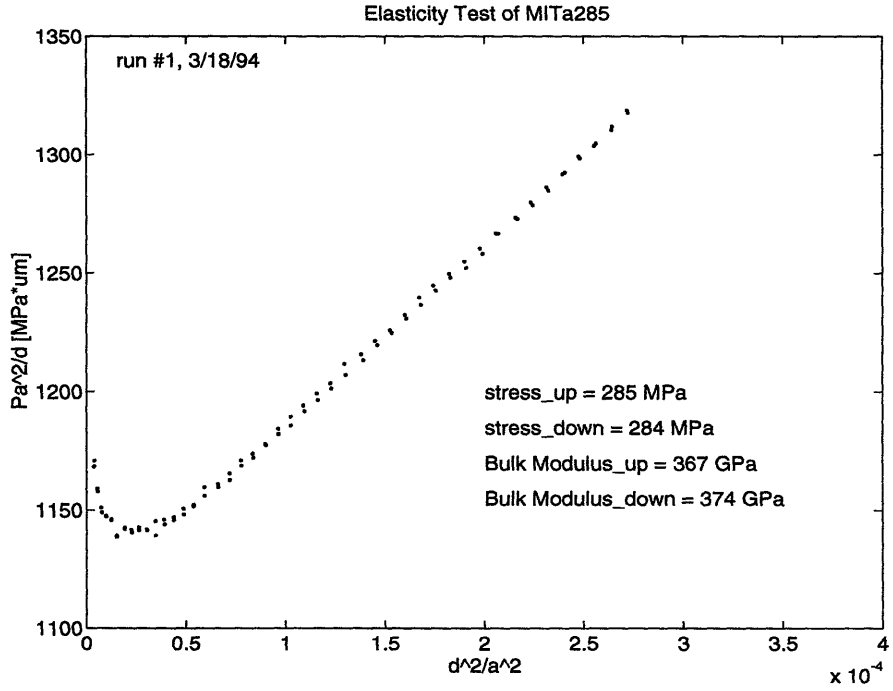

Figure 5.10: Plot used to derive residual stresses and bulk moduli of elasticity test for MITa285

the half of the run with increasing pressure was 285 MPa, while the calculated residual stress from the decreasing pressure part of the run was 284 MPa. The difference in calculated residual stresses is 1 MPa, 0.35% of the increasing part of the run value. The calculated bulk modulus from the increasing pressure part of the run was 367 GPa, while the calculated bulk modulus from the decreasing part of the run was 374 GPa. The difference in bulk moduli was 7 GPa, 1.9% of the increasing pressure part of the run value.

In Figure 5.11 the pressure-deflection curves for a silicon nitride membrane with and without a layer of PMMA deposited on it are shown. For a given pressure, the deflection of the membrane with the PMMA layer is less than the deflection of the membrane without the PMMA layer. The thickness of the membrane was found by the optical transmis-

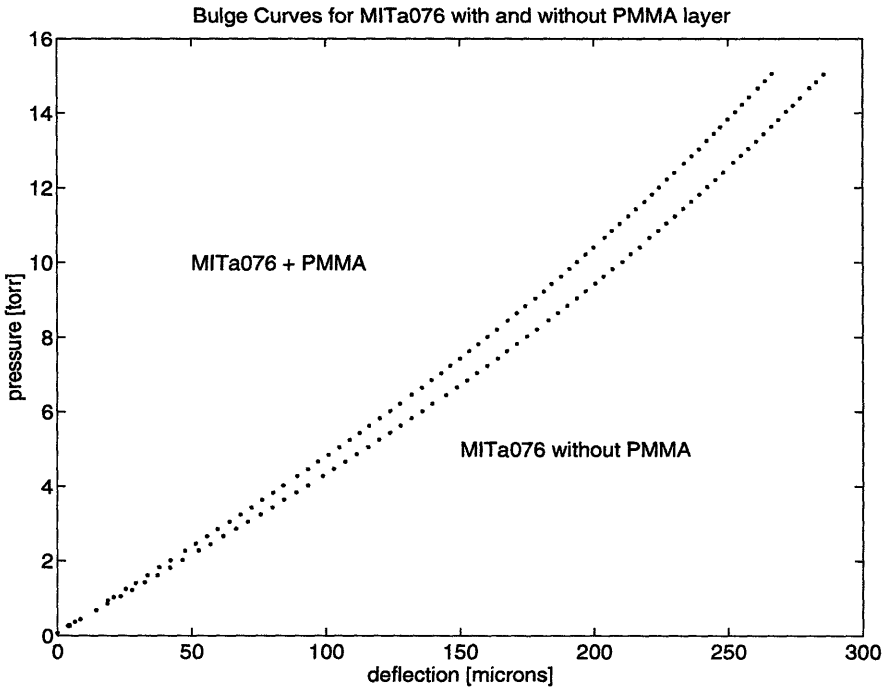

Figure 5.11: Bulge pressure-deflection curves for MITa076 with and without additional PMMA layer

sion test to be 992 nm, and the thickness of the PMMA layer was 1730 nm as found by a

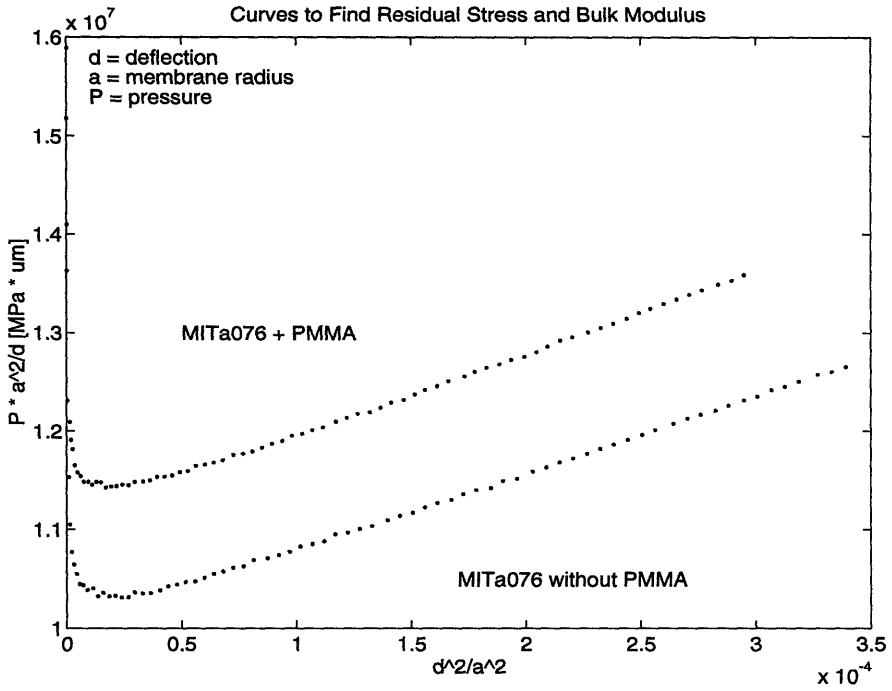

Figure 5.12: Curves to find residual stress and bulk modulus of multilayer sample step edge test under a Linnik interferometer[1]. Using equation (3.51) the residual stress and bulk modulus of the membrane without PMMA were calculated to be 359 +/- 10 MPa and 525 +/- 25 GPa respectively. Using equation (3.55) the residual stress of the PMMA was found to be 22 +/- 6 MPa, and the bulk modulus of the PMMA was calculated as 33 +/- 25 GPa. The errors given are for repeatability and are taken from the repeatability test in Figures 5.7 and 5.8.

1. The deposition and thickness measurement of the PMMA was performed by Scott Hector at the NanoStructures Laboratory.

Chapter 6

Discussion

6.1 Optical Transmission Test

The optical transmission results described in Chapter 5 will be explained in this subsection by using Malé's graphical technique. [24] An expression for the transmitted power in terms of the magnitudes of three vectors will first be found. The reflection coefficients defined in equation (2.7) for the ambient-film-ambient system shown in Figure 2.2 can be expressed in complex polar form as:

$$R_{01} = -\frac{(n_1 + i\alpha_1) - 1}{(n_1 + i\alpha_1) + 1} = -\sigma_1 e^{-i\beta_1} \qquad (6.1)$$

$$R_{12} = \sigma_1 e^{-i\beta_1}$$

We define a vector $\overline{D}$ as:

$$\overline{D} \equiv \frac{1}{R_{01}R_{12}} = \frac{-1}{\sigma_1^2} e^{i2\beta_1} \qquad (6.2)$$

and a vector $\overline{E}$ as:

$$\overline{E} \equiv -exp\,(i4\pi d_1 N_1/\lambda) = -exp\left(-\frac{4\pi\alpha_1 d_1}{\lambda}\right) exp\,(\frac{i4\pi n_1 d_1}{\lambda}) \qquad (6.3)$$

where N_1 is defined in equation (2.16). The value of the transmitted power t can be written as:

$$t = \left|\frac{T_{01}T_{12}}{R_{01}R_{12}}\right|^2 \left|\frac{e^{i2\pi d_1 N_1/\lambda}}{(1/R_{01}R_{12}) + e^{i4\pi d_1 N_1/\lambda}}\right|^2 = K\frac{e^{-4\pi\alpha_1 d_1/\lambda}}{|ED|^2} \qquad (6.4)$$

where ED is shown in Figure 6.1. $T_{l(l+1)}$ is defined in equation (6.5) for a normally incident wave on the film:

$$T_{l(l+1)} = \frac{2N_l}{N_l + N_{(l+1)}} \tag{6.5}$$

where N_i is the refractive index of medium *i*. The variable K in equation (6.4) can be found by using the fact that the transmitted power is equal to one when the film thickness d_1 is equal to zero.

$$K = |E_0 D|^2$$
$$t = \left|\frac{E_0 D}{ED}\right|^2 e^{-4\pi\alpha_1 d_1/\lambda} = \left|\frac{E_0 D}{ED}\right|^2 |E| \tag{6.6}$$

The term E_0D is the distance from D to the point (-1, 0) on the complex plane (which is the value of $\overline{E}$ at d_1 equal to zero). The transmitted power is now expressed in terms of the magnitudes of three vectors shown in Figure 6.1.

The distance ED is strongly dependent on wavelength because of the changes in the angle and magnitude of $\overline{E}$ with wavelength. The values for α_1 and n_1 used in the following analysis were found in fitting the data in Figure 5.1. The magnitude of $\overline{E}$ increases exponentially as wavelength increases until it reaches a steady value at 650 nm as shown in Figure 6.2. The vector $\overline{E}$ encircles the origin and traces a spiral as wavelength increases, as shown in the polar plot in Figure 6.3. The innermost point of the spiral corresponds with 400 nm, and the outermost point of the spiral corresponds with 800 nm.

Many phenomena seen in Figure 5.1 can be explained by the phase, rotation speed, and magnitude of $\overline{E}$ versus wavelength. When $\overline{E}$ is aligned in phase with $\overline{D}$, the distance ED is a minimum causing the transmitted power to have a local maximum. When $\overline{E}$ and $\overline{D}$

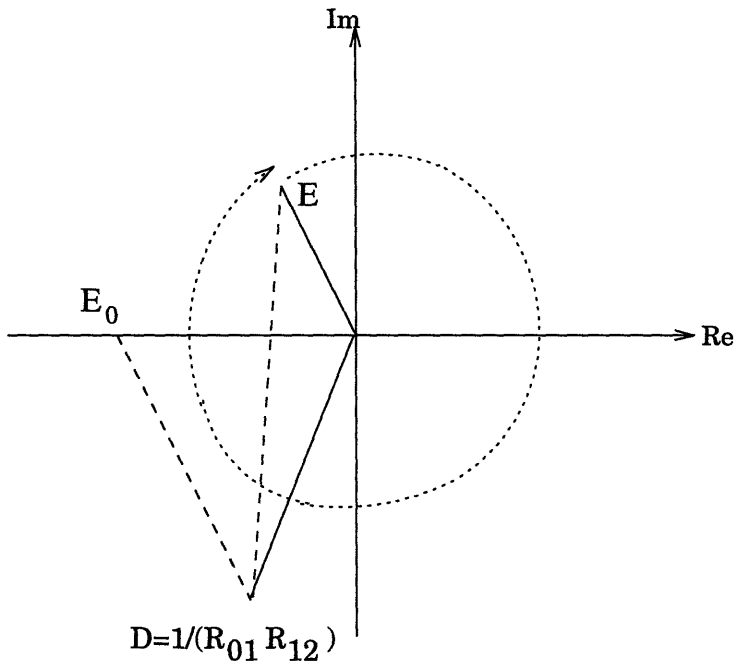

Figure 6.1: Malé's construction for finding the transmitted power of an ambient-film-ambient system

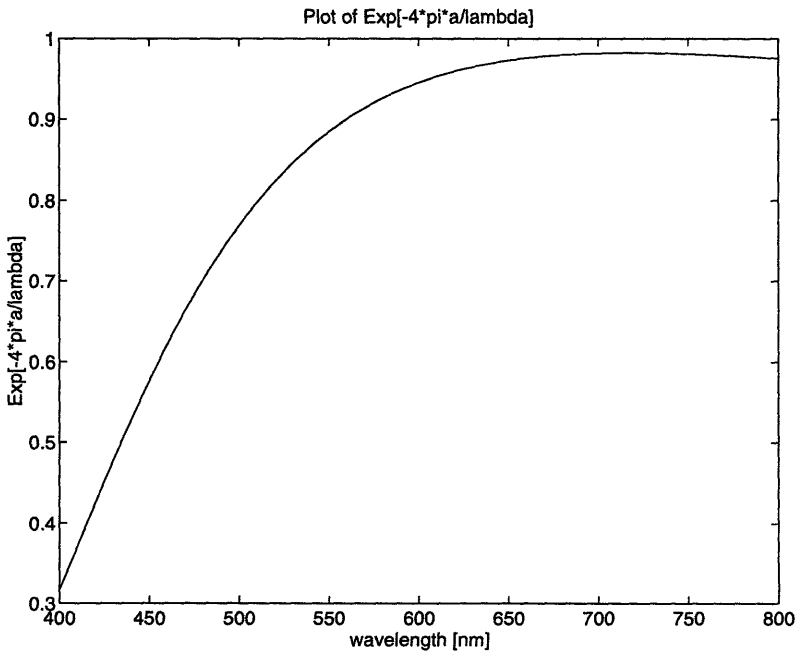

Figure 6.2: Plot of $\exp(-4\pi\alpha d/\lambda)$ versus wavelength

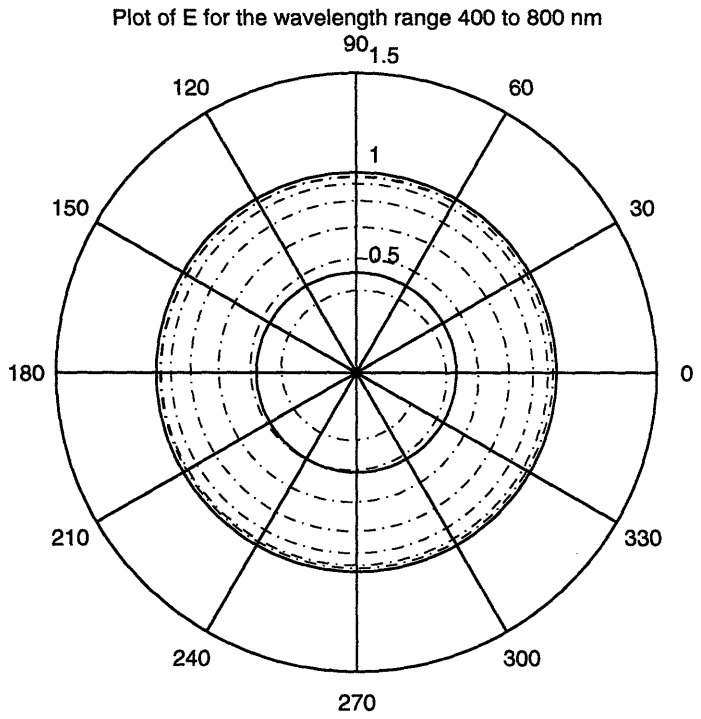

Figure 6.3: Plot of $\overline{E}$ for the wavelength range 400 to 800 nm

are 180 degrees out of phase, the distance ED is a maximum causing the transmitted power to have a local minimum. As $\overline{E}$ revolves around the origin it passes the vector $\overline{D}$ many times, thus the transmitted power goes through a series of maxima and minima as observed in Figures 5.1. As wavelength increases and n_1 decreases, the vector $\overline{E}$ circles the origin at a slower rate, as observed experimentally in the increase in the width of the peaks with increasing wavelength. Above 650 nm the exponential weighting factor in equation (6.6) is roughly constant, and the magnitude of $\overline{E}$ reaches a steady value, thus the transmitted power becomes constant.

6.2 Bulge Test

The observed shape of the bulge test pressure-deflection curves can be explained using equation (3.53). In Figure 5.4, Figure 5.9, and Figure 5.11 the pressure-deflection curves for the silicon nitride membranes were linear up to a deflection of approximately 125

microns and then became nonlinear. Equation (3.53) states that for small deflections the linear term in d dominates, but the nonlinear d^3 term becomes more significant as deflections become large. In Figure 5.11 the slope of the pressure-deflection curve at small deflections was greater for the membrane with the PMMA layer, as expected since the weighting factor of the linear term in d is larger for the multilayer membrane. The nonlinear term in equation (3.53) becomes significant at a slightly lower deflection in the multilayer case in Figure 5.11 than in the single-layer case because of the increased weighting the d^3 term.

The measured values of the residual stress and bulk modulus of silicon nitride correspond roughly to values reported in the literature for different deposition conditions. The measured residual stress of the silicon nitride membrane was 327 +/- 10 MPa, and the measured bulk modulus was 426 +/- 25 GPa. Values of the residual stress and bulk modulus of silicon nitride membranes reported by Bromley were 100 MPa and 190 GPa respectively for a 1 micron thick membrane of radius 5 mm. [9] Bromley used a SiH_2Cl_2:NH_3 gas volume ratio of 5:1 at deposition, while our deposition gas ratio was 10:1. The differences in residual stress and bulk modulus measurements for silicon nitride may be attributed to the difference in deposition conditions.

The residual stress of the deposited PMMA was found to be 22 +/- 6 MPa, and the bulk modulus of the PMMA was 33 +/- 25 GPa. IBM reported the value of the residual stress of PMMA to be 10-20 MPa for a 0.5 micron film using a resonance frequency test. The IBM value is close to our measured value. No reported value of the bulk modulus of PMMA has been found. Our measured value for the bulk modulus of PMMA has very large error bars due to the propagation of the repeatability error in measuring the bulk modulus of the supporting silicon nitride membrane in the multilayer bulge equation.

Several measurement errors were observed in the experimental data. The residual stress and bulk modulus repeatability errors were 3% and 6% of their mean values respectively. In the elasticity test in Figure 5.10 a 1.9% error of the bulk modulus measurement was found between the increasing and decreasing pressure parts of the run, suggesting that a significant part of the error in the bulk modulus measurement is not from clamping or environmental variations. Through examination of the multilayer equation it is seen that a very precise measurement of the deflection is needed in order to achieve a small error bar on the measured bulk modulus since the bulk modulus term is weighted by the cube of the deflection. Figure 5.6 and the deviations from linearity as $(d/a)^2$ goes to zero in Figure 5.10 and 5.12 confirm that there is an error in measuring small deflections with the present bulge test setup.

Chapter 7

Future Work

Modifications to improve the current optical transmission test and bulge test, and two projects related to the optical transmission test and the bulge test are proposed in this chapter. The alterations to the current bulge test setup would decrease the time required for a measurement and would increase the accuracy of the deflection measurements. The optical reflection test would use much of the equipment for the optical transmission test to measure the thickness and refractive index of thin films on a silicon wafer. The in-situ bulge tester for a tungsten sputtering system would provide feedback on the state of the tungsten stress.

7.1 Optical Transmission Test

A more physical model to use for the real and imaginary parts of the index of refraction of a thin absorbing film is the Lorentz harmonic oscillator model. In this model the dielectric constant ε of the thin absorbing film is approximated as the sum of a set of Lorentz oscillators [25]:

$$\varepsilon = \varepsilon_o + \sum_k \alpha_k \left(\frac{1}{h\nu + \beta_k + j\Gamma_k} - \frac{1}{h\nu - \beta_k + j\Gamma_k} \right)$$
$$N_1 = \sqrt{\frac{\mu_o \varepsilon}{\mu_o \varepsilon_o}} = n + i\alpha \tag{7.1}$$

where each oscillator has an amplitude α_k, a center energy β_k, and a broadening factor Γ_k. The Lorentz oscillator model would be an improvement over the model in equation (2.16) since it would prevent the result of the curve fit from being unphysical situation (i.e. determining the absorption coefficient of an absorbing film to be negative).

7.2 Optical Reflection Test

The thickness of thin films deposited on a silicon wafer could be found by measuring the reflected power of the sample over a broad wavelength range. The setup for reflection mode measurements shown in Figure 7.1 uses much of the equipment for the optical transmission test. A beamsplitter at an angle of 45 degrees would direct light towards the sample and subsequently direct the reflected light into the entrance slit of the spectrometer. A mirror below the sample holder would be used to measure the spectrum of the light source.

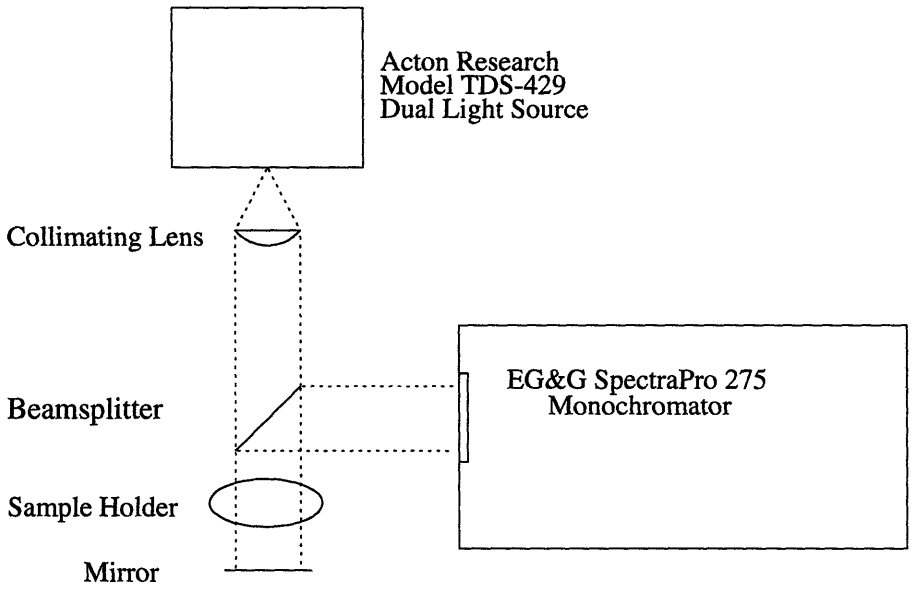

Figure 7.1: Optical reflection test setup

The procedure for reflectance measurements would be similar to the procedure for transmittance measurements. A spectrum of the tungsten light source would be taken and saved in computer memory. A sample would be placed on the sample holder, and the mirror would be covered with a black cloth to prevent multiply reflected and transmitted light from entering the spectrograph. The spectrum with the sample in place would be divided by the spectrum of the light source, resulting in a plot of the reflectance of the sample ver-

sus wavelength. The thickness, and real and imaginary parts of the index of refraction versus wavelength would be found by fitting the reflected power *r* spectrum to:

$$r = \left| (N_1 + N_2)\,(N_1 - N_2) \left[\frac{1 - e^{i2\pi d_1 N_1/\lambda}}{(N_1 + N_2)^2 - (N_1 - N_2)^2 e^{i2\pi d_1 N_1/\lambda}} \right] \right|^2 \quad (7.1)$$

where the expansions for the index of the film N_1 are given in equation (2.16), N_2 is the index of silicon, and d_1 is the thickness of the thin film on the silicon wafer.

7.3 Improvements in the Bulge Test Measurement Schematic

The bulge test measurements are presently a laborious task because of the time required to find the point of highest deflection of the membrane. A set of at least four Fotonic sensors to measure the deflection of the membrane would improve the bulge test measurement scheme by decreasing the time requirement for a measurement and by increasing the accuracy of the deflection measurement. The accuracy would be improved because a measurement of the radius of curvature of the membrane by the set of Fotonic sensors would be a better measurement of the deflection than the point measurement of a single Fotonic sensor. Higher accuracy of the measurement of a single-layer film would decrease the error bars on the measurements of a multilayered sample. The shape of the deflected membrane could also be studied with a set of Fotonic sensors.

7.4 In-Situ Monitoring of the Stress of Sputtered Tungsten

It is possible to deposit low-stress tungsten on x-ray membranes, but it is difficult to achieve good repeatability of the tungsten stress. We propose adding a bulge test in the sputtering system to provide feedback on the current stress of the tungsten. The membrane would be pressurized with a few torr of He gas, which is currently being used in the sput-

tering system to ensure stress and temperature uniformity over the membrane. [26] For small deflections the multilayer bulge equation (3.53) reduces to:

$$P = \frac{4d}{a^2}(\sigma_1 t_1 + \sigma_2 t_2) \tag{7.2}$$

The stress σ_1 and thickness t_1 of the silicon nitride membrane would be measured in the improved ex-situ bulge test before a sputtering run. The thickness t_2 of the sputtered tungsten is currently monitored in the sputtering system, thus the stress of the sputtered tungsten σ_2 could be found using equation (7.2). The argon gas pressure would be adjusted to attain the desired tungsten stress, since the stress of sputtered tungsten has been shown to have a strong dependence on the argon gas pressure.

References

[1] D. L. Spears and H. I. Smith, "X-ray Lithography - A new high resolution replication process", *Solid State Technol.* **15**, No. 7, pp. 21-26, 1972.

[2] R. F. Pease, "Present and future trends in microlithography", *Jpn. J. Appl. Phys.*, Vol. **31**, Pt.1, No. 12B, pp. 4103-4109, 1992.

[3] R. Kumar, T. Ohta, Y. Yamashita, H. Hoga, and K. Koga, "Optically high transparent SiN mask membrane with low stress deposited by low pressure chemical vapor deposition", *Jpn. J. Appl. Phys.*, Vol. **31**, Pt. 1, No. 12B, pp. 4195-4199, 1992.

[4] M. Sekimoto, H. Yoshihara, and T. Okhubo, "Silicon nitride single-layer x-ray mask", *J. Vac. Sci. Technol.*, Vol. **21**, No. 4, pp. 1017-1021, 1982.

[5] M. Karnezos, "Effects of stress on the stability of x-ray masks", *J. Vac. Sci. Technol. B*, Vol. **4**, No. 1, 1986, pp. 226-229, 1986.

[6] M. Oda, S. Ohki, A. Ozawa, T. Ohkubo, and H. Yoshihara, "Simulation of x-ray mask distortion", *Jpn. J. Appl. Phys.*, Vol. **31**, Pt. 1, No. 12B, pp. 4189-4194, 1992.

[7] A. W. Yanof, D. J. Resnick, C. A. Jankoski, and W. A. Johnson, "X-ray mask distortion: process and pattern dependence", *SPIE Vol.* **632** *Electron-Beam, X-Ray, & Ion-Beam techniques for Submicrometer Lithographies V*, pp. 118-131, 1986.

[8] J. W. Beams, "Mechanical properties of thin films of gold and silver", in *Structure and Properties of Thin Films*, edited by C. A. Neugebauer, J. B. Newkirk, and D. A. Vermilyea, New York: John Wiley and Sons, pp. 183-192, 1959.

[9] E. I. Bromley, J. N. Randall, D. C. Flanders, and R. W. Mountain, "A technique for the determination of stress in thin films", *J. Vac. Sci. Technol. B* **1** (4), pp. 1364-1366, 1983.

[10] G. F. Cardinale and R. W. Tustison, "Mechanical property measurement of polycrystalline diamond films", *SPIE Vol.* **1325** *Diamond Optics III*, pp. 90-98, 1990.

[11] G. F. Cardinale and R. W. Tustison, "Fracture strength and biaxial modulus measurement of plasma silicon nitride films", *Thin Solid Films* **207**, pp. 126-130, 1992.

[12] R. J. Jaccodine and W. A. Schlegel, "Measurement of strains at Si-SiO2 interface", *Journal of Applied Physics*, Vol. **37**, No. 6, pp. 2429-2434, 1966.

[13] P. Lin, Ph.D. Thesis, M. I. T., 1990.

[14] J. Pan, Ph.D. Thesis, M. I. T., 1991.

[15] M. K. Small and W. D. Nix, "Analysis of the accuracy of the bulge test in determining the mechanical properties of thin films", *J. Mater. Res.*, Vol. **7**, No. 6, pp. 1553-1563, 1992.

[16] F. Tsai, B.S. Thesis, M. I. T., 1991.

[17] T. Tsakalakos, "The bulge test: a comparison of theory and experiment for isotropic and anisotropic films", *Thin Solid Films*, Vol. **75**, pp. 293-305, 1981.

[18] J. A. Kong, *Electromagnetic Wave Theory.* New York: Wiley, pp. 120-133, 1986.

[19] R. T. Fenner, *Mechanics of Solids.* Oxford: Blackwell Scientific Publications, 1989, Chapters 1-3.

[20] T. J. Lardner, ed. *An Introduction to the Mechanics of Solids.* New York: McGraw-Hill Book Company, 1972, Chapters 4-5.

[21] S. P. Timoshenko, *Theory of Elasticity.* New York: McGraw-Hill Book Co., 1970, pp. 244-248.

[22] K. Washizu, *Variational Methods in Elasticity and Plasticity.* Oxford: Pergamon Press, 1968, pp. 27-29.

[23] S. Timoshenko, *Theory of Plates and Shells.* New York: McGraw-Hill, 1940, p. 329.

[24] O. S. Heavens, *Optical Properties of Thin Solid Films.* New York: Dover Publications, Inc., 1965, pp. 82-89.

[25] J. A. Woollam, P. G. Snyder, and H. Yao, "In-situ and ex-situ ellipsometric characterization for semiconductor technology", *SPIE Vol.* **1678**, pp. 246-257, 1992.

[26] H. Li, M.Eng. Thesis, M. I. T., 1994.

Appendix A

Optical Transmission Test Computer Programs

The optical transmission test program consists of two programs. The program runner(file) runs the runs the transmission fitt for the data in "file". The program transmission(parameters) contains equation (2.15) for the transmitted power of the ambient-film-ambient system shown in Figure 2.2. The Levenberg-Marquardt fitting algorithim is used to find the best fit to the experimental data.

A.8 Runner(file)

```
function parameters = runner(file)
%RUNNER(FILE)                runs the transmission fitting program with the
%                            data in FILE; uses the Levenberg-Marquardt
%                            least squares fitting algorithim

global Plothandle lambda transmission parameters

lambdan = file(:,1);                %lambda is 1st column of FILE
lambda = lambdan(200:5:600);
transmissionn = file(:,2);          %transmission is 2nd column of FILE
transmission = transmissionn(200:5:600);

plot(lambdan, transmissionn, 'm-')  %plot original data
xlabel('wavelength (nanometers)')
ylabel('transmission')
title('Transmission Fit')
hold on

%plot fit line which will move as the fit progresses
Plothandle = plot(lambda, transmission, 'c--', 'EraseMode', 'xor');

%initial guess
start = [970.4261 2.1145 1.5249e4 3.6798e9 0.0332 -33.4289 5.6137e6]';

options(2) = 0.02;                  %termination criteria for parameters
options(14) = 400;                  %maximum number of iterations

parameters = leastsq('transmission', start, options);
```

```
d = parameters(1);
n0 = parameters(2);
n2 = parameters(3);
n4 = parameters(4);
k0 = parameters(5);
k1 = parameters(6);
k3 = parameters(7);

lamHeNe = 632.8;                    %find values of n and k at the HeNe wavelength
nHeNe = n0 + n2 /(lamHeNe)^2 + n4/(lamHeNe)^4;
kHeNe = k0 + k1/lamHeNe + k3/(lamHeNe)^3;

%print values of d, nHeNe, and kHeNe on screen
dstring = sprintf('thickness = %5.4g nm', d);
nstring = sprintf('n(632.8) = %.4f', nHeNe);
kstring = sprintf('k(632.8) = %.5f', kHeNe);
text(lambda(50), 0.4, dstring)
text(lambda(50), 0.3, nstring)
text(lambda(50), 0.2, kstring)
```

A.9 Transmission(parameters)

```
function error = transmission(parameters)
%TRANSMISSION                       plots transmission of an ambient-film-ambient
%                                   system using complex arithmetic
global Plothandle lambda transmission error

d = parameters(1);
n0 = parameters(2);
n2 = parameters(3);
n4 = parameters(4);
k0 = parameters(5);
k1 = parameters(6);
k3 = parameters(7);

%define polynomial expansions for n and k
n = n0 + n2 ./ (lambda).^2 + n4 ./(lambda).^4;
k = k0 + k1 ./ lambda + k3 ./(lambda).^3;
N = n - j*k;
beta = 2 * pi * d * N ./ lambda;

%calculate Fresnel reflection and transmission coefficients
t01 = 2 ./ (1 + N);
t12 = 2 * N ./ ( 1 + N);
r01 = (N - 1) ./(1 + N);
r12 = (1 - N) ./ (1 + N);
```

```
%calculate transmitted power
Tnum = t01 .* t12 .* exp(-j * beta);
Tden = 1 + r01 .* r12 .* exp(-2 * j * beta);
t = abs(Tnum ./ Tden) .* abs(Tnum ./ Tden);

set(Plothandle, 'ydata', t)
drawnow

error = t - transmission;                %error of fit
hold off
```

Appendix B

LabVIEW Computer Programs

The heart of the LabVIEW programs for the bulge test measurement system are shown on the following pages. On page 66 the main bulge test driver is shown, and the subVIs which the main program calls are shown on pages 67 - 69. On page 67 the subVI which acquires, filters, and averages the data is shown. On page 68 the subVI which does a linear fit of the data is shown. Finally on page 69 the subVI which translates the slope and intercept of the linear fit into the residual stress and bulk modulus of the tested membrane layer is shown.

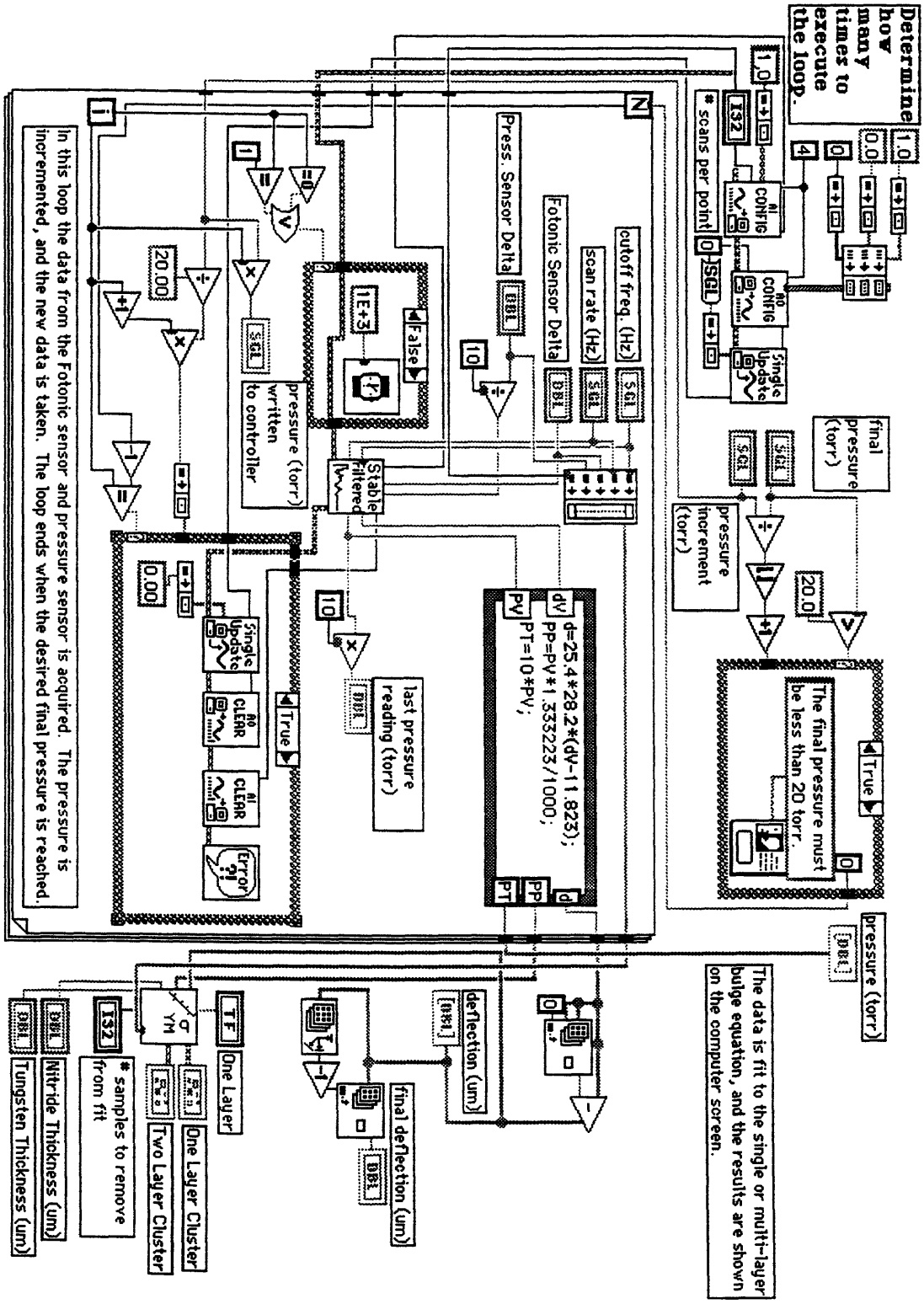
Determine how many times to execute the loop.
final pressure (torr)
pressure increment (torr)
The final pressure must be less than 20 torr.
pressure (torr)
The data is fit to the single or multi-layer bulge equation, and the results are shown on the computer screen.
cutoff freq. (Hz)
scan rate (Hz)
Fotonic Sensor Delta
Press. Sensor Delta
pressure (torr) written to controller
Stable Filtered
last pressure reading (torr)
d=25.4*28.2*(dV-11.823);
PP=PV*1.333223/1000;
PT=10*PV;
deflection (um)
final deflection (um)
One Layer
One Layer Cluster
Two Layer Cluster
* samples to remove from fit
Nitride Thickness (um)
Tungsten Thickness (um)
In this loop the data from the Fotonic sensor and pressure sensor is acquired. The pressure is incremented, and the new data is taken. The loop ends when the desired final pressure is reached.

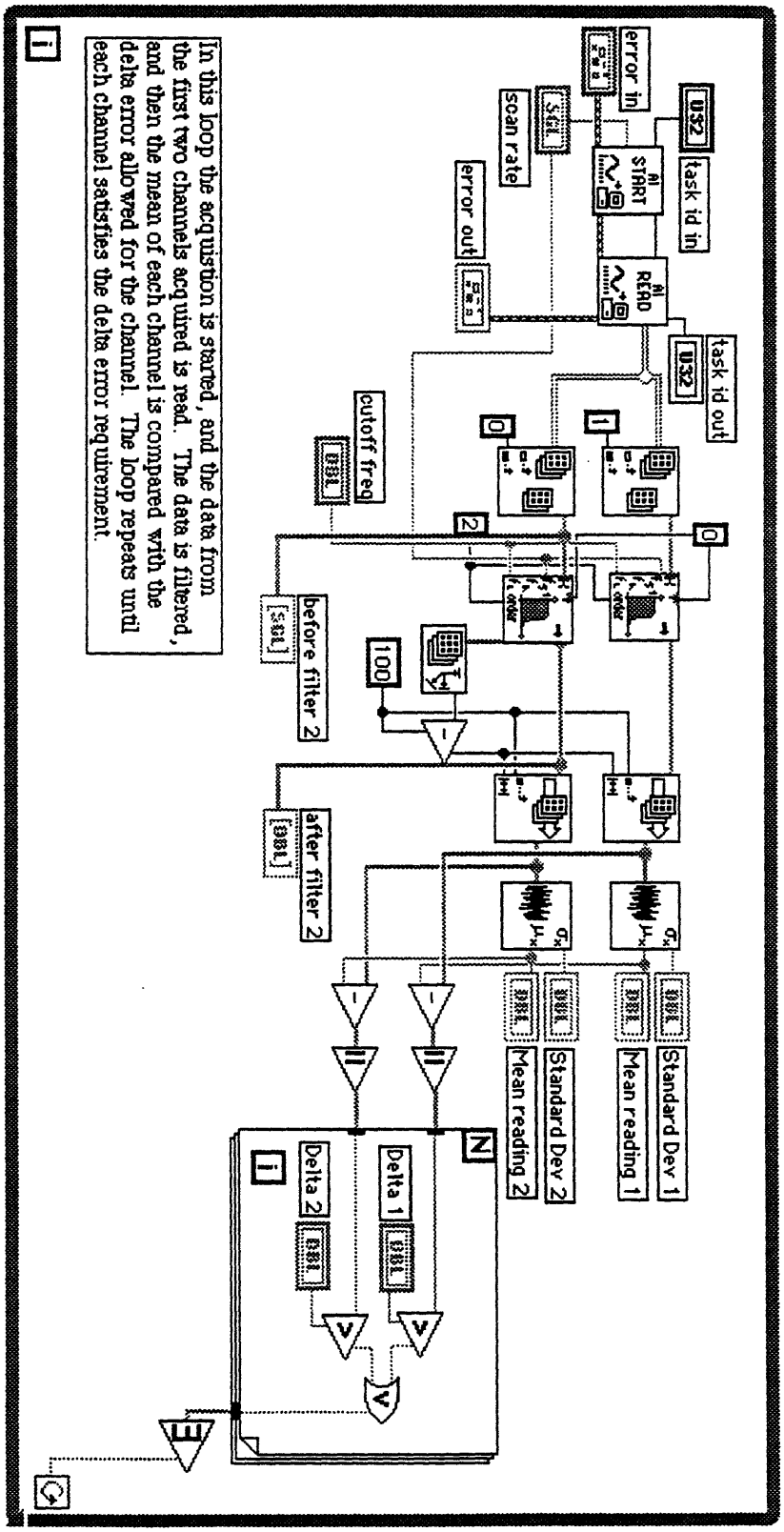
In this loop the acquistion is started, and the data from the first two channels acquired is read. The data is filtered, and then the mean of each channel is compared with the delta error allowed for the channel. The loop repeats until each channel satisfies the delta error requirement.
error in
task id in
scan rate
error out
task id out
cutoff freq
before filter 2
after filter 2
100
Standard Dev 1
Mean reading 1
Standard Dev 2
Mean reading 2
Delta 1
Delta 2

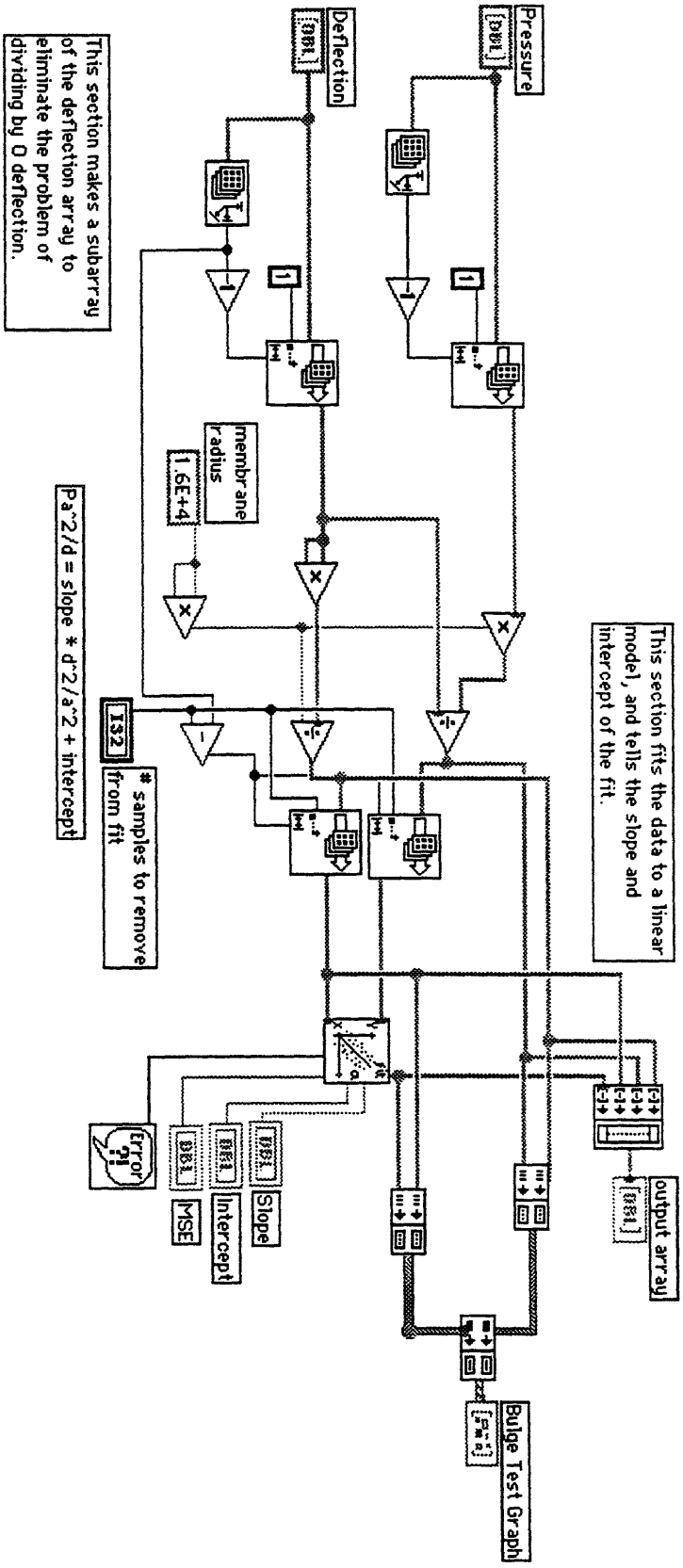
Pressure
Deflection
membrane radius
1.6E+4
This section makes a subarray of the deflection array to eliminate the problem of dividing by 0 deflection.
Pa^2/d = slope * d^2/a^2 + intercept
This section fits the data to a linear model, and tells the slope and intercept of the fit.
132
samples to remove from fit
output array
Error
MSE
Intercept
Slope
Bulge Test Graph

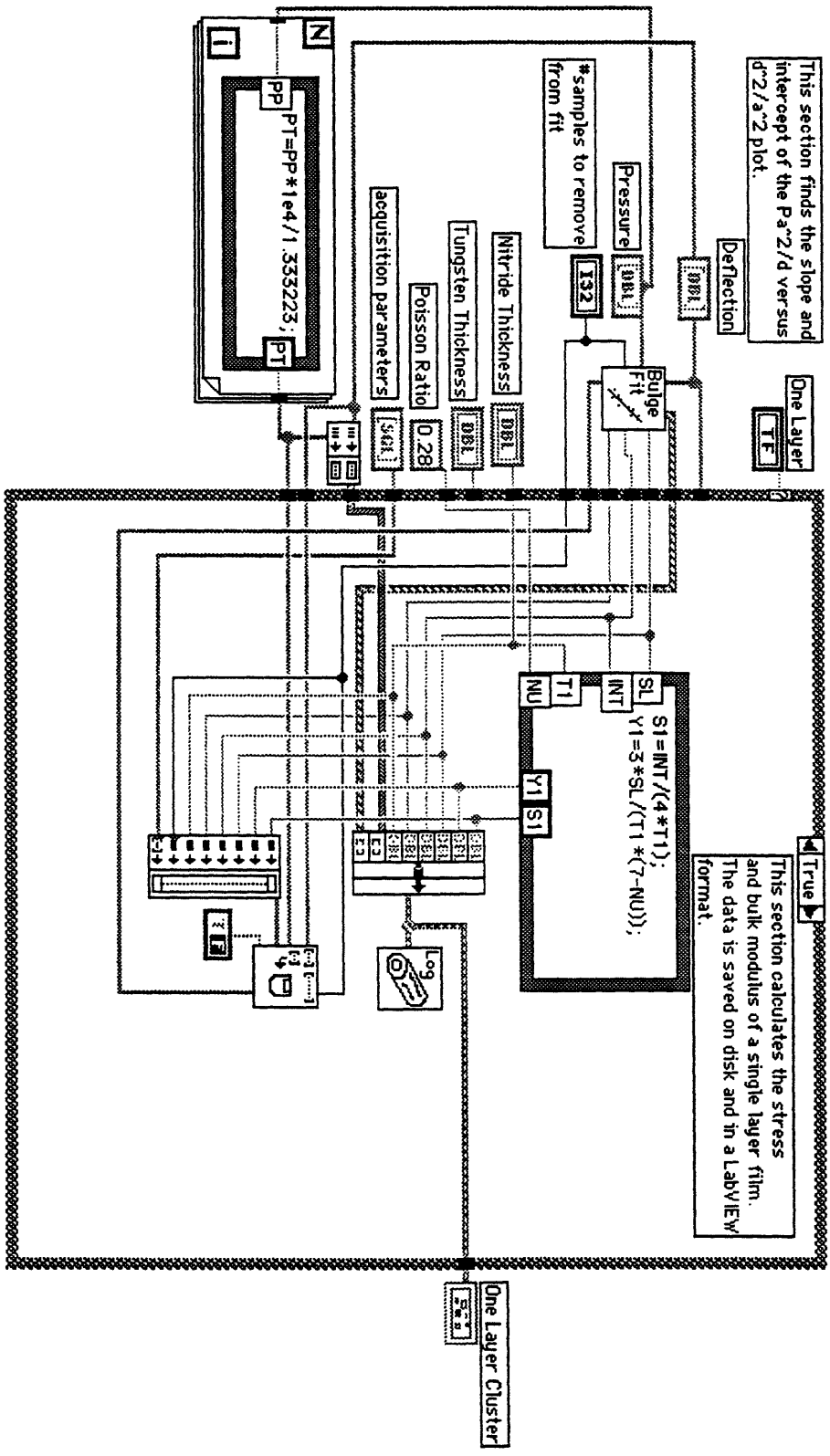
This section finds the slope and intercept of the Pa^2/d versus d^2/a^2 plot.
Deflection
Pressure
#samples to remove from fit
I32
Bulge Fit
One Layer
TF
Nitride Thickness
Tungsten Thickness
Poisson Ratio
0.28
acquisition parameters
N
i
PP
PT=PP*1e4/1.333223;
PT
SL
INT
T1
NU
S1=INT/(4*T1);
Y1=3*SL/(T1*(7-NU));
Y1
S1
True
This section calculates the stress and bulk modulus of a single layer film. The data is saved on disk and in a LabVIEW format.
Log
One Layer Cluster